Draft version February 9, 2011
Preprint typeset using LaTeX style emulateapj v. 11/10/09

"SPECTROSCOPIC DETERMINATION OF THE LOW REDSHIFT TYPE IA SUPERNOVA RATE FROM THE SLOAN DIGITAL SKY SURVEY"

K. Simon Krughoff[1], Andrew J. Connolly[1], Joshua Frieman[2,3], Mark SubbaRao[4,5], Gary Kilper[6], and Donald P. Schneider[7]

Draft version February 9, 2011

ABSTRACT

Supernova rates are directly coupled to high mass stellar birth and evolution. As such, they are one of the few direct measures of the history of cosmic stellar evolution. In this paper we describe an probabilistic technique for identifying supernovae within spectroscopic samples of galaxies. We present a study of 52 type Ia supernovae ranging in age from -14 days to +40 days extracted from a parent sample of $\sim$ 350,000 spectra from the SDSS DR5. We find a Supernova Rate (SNR) of $0.472^{+0.048}_{-0.039}(Systematic)^{+0.081}_{-0.071}(Statistical)SNu$ at a redshift of $\langle z \rangle = 0.1$. This value is higher than other values at low redshift at the 1σ, but is consistent at the 3σ level. The 52 supernova candidates used in this study comprise the third largest sample of supernovae used in a type Ia rate determination to date. In this paper we demonstrate the potential for the described approach for detecting supernovae in future spectroscopic surveys.

1. INTRODUCTION

Over the last decade, the study of the properties of type Ia supernovae (abbreviated SNe in captions and equations) has become one of the fundamental tools used in observational cosmology. With peak luminosities on the order of $M_V \sim -19.3$, type Ia supernovae can be observed out to redshifts of $z > 1$. This enables a broad range of science: enrichment of the interstellar medium (Sivanandam et al. 2009), characterization of the expansion history of the Universe (Schmidt et al. 1998; Perlmutter et al. 1999), and understanding the physics of how progenitors transition into supernovae (Mannucci et al. 2006). This scientific potential has led to the a number of surveys of supernovae in the local and distant universe (Wood-Vasey et al. 2004; Pritchet & For The Snls Collaboration 2005; Hamuy et al. 2006; Miknaitis et al. 2007; Frieman et al. 2008; Hicken et al. 2009).

The primary method for detecting and characterizing supernovae is through repeated imaging of the same region of the sky spread over several months or years. By difference imaging multiple epochs (Alard & Lupton 1998), host galaxies can be subtracted, revealing candidate supernovae that can then be classified by additional imaging or spectroscopy. Madgwick et al. (2003) demonstrated that supernovae can also be identified in an analogous way from spectroscopic observations by subtracting the underlying host galaxy spectrum. In this case the detection and classification of the supernova can be derived from a single observation; with a direct measure of the redshift, type and age of the supernova. While less efficient than imaging techniques (as the observational cost of obtaining the spectroscopic data is much larger) this approach can be applied serendipitously to any spectroscopic survey to study, for example, supernovae rates in the local and distant universe.

Madgwick et al. (2003) found a local supernovae rate of $R_{Ia}(z \leq 0.25) = 0.4 \pm h^2 SNu$[8], which is consistent with existing measures but was based on only 19 supernovae. In this paper we expand upon this work to undertake a systematic study of type Ia supernovae as found in the SDSS main galaxy sample. We consider the statistical and systematic uncertainties that arise when classifying supernovae from the SDSS spectra, the efficiency of the detection technique (as a function of redshift, galaxy type and signal-to-noise ratio) and discuss ways to minimize the impact of systematics due to misclassification of narrow and broad emission-line galaxies. Applying these techniques to the 362,431 spectra from the SDSS DR5 sample we characterize the supernova population and supernova rates for redshifts $z < 0.1$. For calculations dependent on cosmology, we use $\Omega_m = 0.3$, $\Omega_\Lambda = 0.7$, and $H_o = 70 kms^{-1}Mpc^{-1}$ throughout this paper.

2. SPECTROSCOPIC SAMPLES

Throughout this paper, we use galaxy samples based on the DR5 (Adelman-McCarthy et al. 2007) release of the SDSS. The SDSS spectra are observed through 3" diameter fibers using a multi-object spectrograph with a spectral resolution of R $\simeq$ 1800 and a wavelength range of 3800 – 9200 Å. Galaxy spectroscopic target selection (Strauss et al. 2002) is based on imaging from the SDSS camera (Gunn et al. 1998) using the 2.5m telescope (Gunn et al. 2006) at Apache Point Observatory. A discussion of the photometric and spec-

[1] Department of Astronomy, University of Washington, Box 351580, Seattle, WA 98195-1580, USA
[2] Fermi National Accelerator Laboratory, P.O. Box 500, Batavia, IL 60510, USA
[3] Kavli Institute for Cosmological Physics and Department of Astronomy and Astrophysics, University of Chicago, 5640 South Ellis Avenue, Chicago, IL 60637, USA
[4] Department of Astronomy and Astrophysics, University of Chicago, 5640 South Ellis Avenue, Chicago, IL 60637.
[5] Adler Planetarium and Astronomy Museum, Chicago, IL 60605.
[6] NASA Goddard Space Flight Center, Code 671, Greenbelt, MD, 20771
[7] Department of Astronomy and Astrophysics, 408A Davey Laboratory, University Park, Pennsylvania 16802

[8] $SNu = 1/10^{10} L_{B\odot}/100yr$ is the definition for the B-band weighted supernova rate used throughout this paper.

troscopic pipelines and the spectrophotometric calibration can be found in Stoughton et al. (2002). The SDSS photometric system is described in detail in Fukugita et al. (1996), Hogg et al. (2001), Smith et al. (2002), Ivezić et al. (2004), Tucker et al. (2006), and Padmanabhan et al. (2008); the filter response curves are given in Fukugita et al. (1996). The astrometric calibration is described in Pier et al. (2003).

For the purpose of this work, we assume that the SDSS spectra have accurate relative spectrophotometric calibration. Discussion of the quality of the SDSS spectrophotometric calibration can be found in Adelman-McCarthy et al. (2007). For this paper, however, we note that the rms dispersion in the absolute spectrophotometry for the SDSS is $\sigma = 0.04$ mag based on the differences between photometric fiber magnitudes and magnitudes synthesized from the SDSS spectroscopy ([9]) and that, at worst, the spectra show a 5% variation in the relative spectrophotometric calibration at the blue end of the spectrum. All spectra are shifted to the restframe and corrected for Galactic extinction using the dust maps of Schlegel et al. (1998) and applying the reddening spectrum from Cardelli et al. (1989) with near ultraviolet updates by O'Donnell (1994). The spectra are re-sampled to 3 Å linear bins to match the resolution of the available supernova templates.

Two galaxy samples were constructed for use in this paper (see Table 1 for a synopsis of these samples). We applied the following criteria to the 1048960 spectra in the DR5 database: a redshift limit of $z < 0.2$, a positive redshift, and the requirement that type derived from the spectrum was not "STAR". The redshift limit for these data was applied in order to exclude the high redshift luminous red galaxy (LRG) population. We wish to avoid segments of the sample dominated by LRGs as this population would have significantly different eigen spectra compared to the low redshift galaxy sample.

Further we define a statistical sample for use in determining the cosmic supernova rate using the selection criteria used to create the Pitt-CMU Value Added Catalog (VAC; [10]). In the SDSS, each observed spectrum has a set of binary flags set either by the data acquisition system or the reduction pipeline. The statistical sample was assembled using the flags associated with the redshift measurement of the object. These redshift flags being set can indicate problems with the spectrum and are for this reason eliminated from the sample. See Stoughton et al. (2002) for complete descriptions of the flags. These criteria are:

1. Spectroscopically classed as a galaxy (SPECCLASS = 2)
2. The following redshift flags are set to zero: Z_WARNING_LOC – Confidence is low, Z_WARNING_NO_SPEC – No spectrum, Z_WARNING_NO_BLUE – No blue side spectrum, and Z_WARNING_NO_RED – No red side spectrum
3. Redshift status flags not set to 0 or 1 (0 = not measured, 1 = failed)
4. Redshift confidence level greater than 70%
5. The spectrum is the highest S/N example of the object

This statistical sample contains 362,431 unique objects. We note that these criteria are less strict than those employed in building the SDSS Main Galaxy sample (Strauss et al. 2002) and provides more objects for analysis. All derived attributes (e.g. apparent magnitudes, absolute magnitudes, and signal to noise measurements) are taken from the VAC. In the redshift range $0.01 < z < 0.2$ the VAC is 4% larger than the Main sample using the same criteria. Although the two samples are selected using different criteria, a contributing factor to the VAC being larger is that the Main sample is magnitude limited to $m_{fiber_r} < 19.0$ where the VAC has no such limit.

We randomly select a subset of galaxies from the statistical sample to determine the efficiency and systematics of the supernova detection and classification method. No attempt was made to avoid spectra with supernova contribution already present. This should not, however, affect efficiency or systematics estimates, since only 0.025% of galaxies are expected to contain a supernova. The model sample is constructed by randomly selecting two thirds of the runs in the DR5 release which provides enough galaxies to capture the statistical properties of the statistical sample but saves compute and storage resources. This model sample consists of 234638 galaxies.

For each galaxy in the model sample a type Ia supernova template is added to the galaxy spectrum (with the supernova age chosen at random from an interval of -20 to +50 days from peak brightness). The absolute luminosity of the supernova is sampled from the distribution of B-band peak brightnesses given in Dahlen et al. (2004). The luminosity is scaled to the observation time using the parametrization of the lightcurve introduced in Goldhaber et al. (2001). We assume a stretch factor $s = 1$ for all synthetic supernovae. The spectra are then shifted and dimmed based on the redshift of the host galaxy. Host galaxy extinction and reddening is applied by choosing a V-band absorption in magnitudes, A_V, from an exponential distribution, $P(A_V) = e^{(-A_V/m)}$, with the scaling parameter, $m = 0.33 \pm 0.09$, and using an Cardelli et al. (1989) reddening curve with updates to the near ultraviolet by O'Donnell (1994). Galactic reddening is applied using the Schlegel et al. (1998) Galactic reddening maps again assuming a Cardelli et al. (1989) with O'Donnell (1994) reddening curve. We do not attempt to correlate supernova properties with host spectral properties.

3. METHOD

As described in Madgwick et al. (2003), our goal is to identify supernova within SDSS spectra. In this section we describe our extension of the initial work of Madgwick et al. (2003). We approach this problem by requiring that our technique must satisfy the following attributes:

1. Computational Efficiency: It must be computationally tractable to classify spectra in real time.
2. Efficient and Complete Detection: Detection must produce few false positives and reject none of the

[9] http://www.sdss.org/DR6/products/spectra/spectrophotometry.html
[10] http://nvogre.astro.washington.edu/vac

candidates with more than four matched spectral features above the noise in the spectrum.

3. Quantifiable Selection Effects: No method will be exact, but to be useful, the method must have uncertainties which can be quantified.

Principal component analysis (PCA) of galaxy spectra has shown that, in the visible regime, spectral energy distributions are inherently low dimensional (Connolly et al. 1995; Folkes et al. 1996; Yip et al. 2004a). The spectra can, therefore, be represented by a small set of orthogonal components or eigen spectra. Yip et al. (2004a) demonstrated that between eight and eleven components are sufficient to describe fully the spectral variation within galaxy spectra in the Sloan Digital Sky Survey (SDSS;York et al. (2000)). This results in a reduction in the complexity or dimensionality of the spectroscopic data by a factor of 400 and means that it is computationally tractable to fit host galaxy spectra jointly with any additional components (e.g. template supernovae Ia spectra). Alternative approaches such as fitting a spectral synthesis model (e.g. (Bruzual & Charlot 2003)) can be computationally expensive due to the breadth of the phase space that must be searched.

Based on the PCA approach we express each spectrum as a linear combination of eigen spectra, e_{ij}, scaled by an expansion coefficient, a_i, where j indexes the wavelength bins. In this way the spectrum, f_j is represented by,

$$\hat{f}_j = \sum_{i=0}^{n-1} a_i e_{ij} \quad (1)$$

where n is the number of spectral eigencomponents used. If the number of spectral components is less than the dimensionality of the data, the reconstructed spectrum is said to be a "lossy" compression. However, as the PCA is a variance weighted statistic, this truncated expansion preferentially suppresses the noise within a spectrum.

We use the first eight ($n = 8$) eigen spectra from Yip et al. (2004a) to fit the galaxy contribution. Figure 1 shows the first six galaxy eigen spectra and the two QSO eigen spectra used in the fitting. At this level of truncation the contribution from higher order eigen spectra is typically less than 1% of the total flux.

From this expansion we calculate the error weighted log likelihood ($log(L)$) value for each spectrum.

$$log(L) = \sum_{j=0}^{m} (f_j - \hat{f}_j)/\sigma_j^2 \quad (2)$$

where f_j and $\hat{f}_j$ are the spectrum flux and reconstructed flux, respectively, and σ_j is the rms error as a function of wavelength.

To determine the best fit supernova spectrum, we refit each SED using the same eigen spectra together with a series of supernovae templates taken from Nugent et al. (1997). These 91 supernova templates range in age, defined as the rest frame time from peak brightness, from -20 days to +70 days. Example supernova templates are shown in Figure 2. For each of the supernova templates, we recalculate the $log(L)$ value and take the minimum

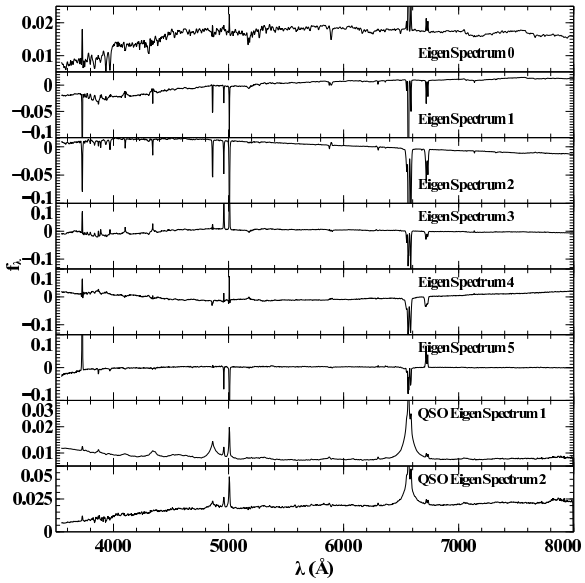

FIG. 1.— First six galaxy eigen spectra and the two QSO eigen spectra used in the fits of our galaxy sample. The top most spectrum is the mean spectrum. The spectra have been re-sampled to 3Å linear bins.

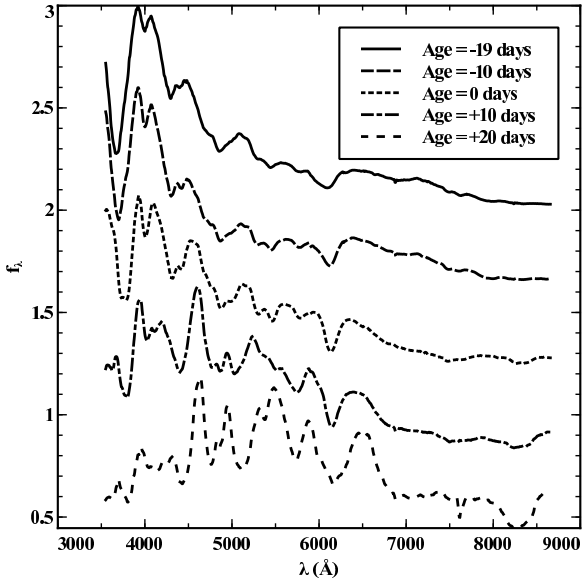

FIG. 2.— Example SN templates from Nugent et al. (1997) at various ages. Spectra have been offset for clarity.

$log(L)$ to be the best fit age. An example of this procedure is shown in Figure 3 together with the resulting residuals after subtracting the galaxy model.

In cases where there is strong nuclear activity, the galaxy eigen spectra under fit broad emission line features. Due to a conspiracy between SiII and OI absorption, type Ia supernova spectra (Branch et al. 1982) produce an apparent emission feature at ~ 6500 Å. This effect creates false positives from confusion between this absorption feature and broad Hα emission in type 1 Seyfert-like galaxies. Even though the fraction of AGN is small (5%-10%), this leads to several tens of thousands of false positives. We therefore include an additional component in the galaxy model based on the first two QSO eigen spectra from Yip et al. (2004b). The QSO compo-

nent fits the broad and narrow emission which decreases the number of false positives by an order of magnitude.

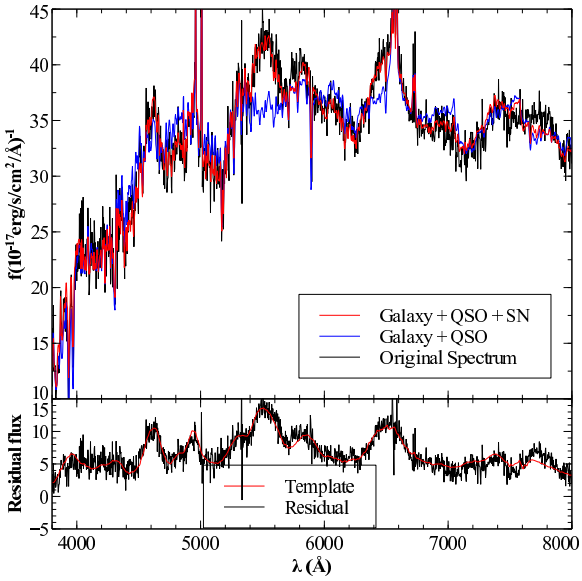

FIG. 3.— Comparison of the fits with only galaxy eigen spectra (blue line) and eigen spectra with a supernova template (red line) for a spectrum with significant supernova contribution (SDSS J083909.65+072431.6). The original spectrum is shown in black. The residual supernova signal from the top pane (Observed-(Galaxy + QSO)). Note that the flux contribution from the supernova is greater than 50% that of the galaxy. The residual is shown in black with the best fit supernova template in red.

3.1. *Selection Criteria for supernova Candidates*

To determine the low redshift supernova rate, we must discriminate reliably between those galaxy spectra that contain supernovae and those that do not. To accomplish this we consider two measures of the significance of a supernova detection: the signal-to-noise of the residual flux after subtraction of the galaxy and QSO components, and the goodness of fit of the supernova template measured by Equation 2 when the flux is estimated using all eigen spectra plus the best fit supernova template.

We define the signal-to-noise as

$$\frac{S}{N} = \frac{\sum_{j=4500\mathring{A}}^{6000\mathring{A}} R_j}{\sqrt{\sum_{j=4500\mathring{A}}^{6000\mathring{A}} \sigma_j^2}}, \quad (3)$$

where $R_j = f_j - \sum_{i=0}^{n} a_i e_{ij}$ is the residual flux after subtracting the underlying galaxy and QSO components, and n is the number of eigen spectra used to model the galaxy and QSO spectra (in our case the first two QSO components were used). The signal-to-noise is measured over the wavelength interval 4500Å – 6000Å in order to exclude contamination of the flux due to Hα.

Following the method outlined in Richards et al. (2004), we use a nonparametric Bayes classifier (NBC) to select supernova candidates. For a general two class system the NBC can be written as:

$$P(C_1|x) = \frac{p(x|C_1)P(C_1)}{p(x|C_1)P(C_1) + p(x|C_2)P(C_2)} \quad (4)$$

For our problem, C_1 is the supernova candidate class (SN), and C_2 is the class of galaxies without supernovae (GAL). The variable x is the two dimensional location of a source within the $\frac{S}{N}$ – $log(L)$ space. The priors $P(C_1)$ and $P(C_2)$ are the probability of drawing a galaxy with a supernova ($P(SN)$) and without a supernova ($P(GAL)$) respectively. We choose $P(SN) = 3/10000$. This value is consistent with estimates from historical supernova rate calculations and with the numbers we see when the algorithm is run on the statistical sample. This is a two class system so, $P(GAL) = 1 - P(SN)$.

We estimate the relative likelihoods for the NBC using the Statistical and Model samples described in the previous section. Figure 4 shows the probability density distributions of the Statistical and Model samples within the $\frac{S}{N}$ – $log(L)$ space. White corresponds to high probability density and black low probability density. Overlaid on these plots are contours of the value of $P(SN|\frac{S}{N}, log(L))$ corresponding to 3, 4, and 5σ confidence levels that a source contains a supernova.

Probability density functions for the samples have been estimated by fitting a mixture of Gaussians using the FastMix package (Moore (1998)). The probability $P(SN|x)$ is then derived from $P(\frac{S}{N}, log(L)|GAL)$, and $P(\frac{S}{N}, log(L)|SN)$. For our current work we choose to classify a galaxy as a supernova candidate if $P(SN|\frac{S}{N}, log(L)) \geq 0.9973$. This corresponds to a 3σ threshold. We further define a subset of supernovae the bronze, silver, and gold candidates (see Section 5) using thresholds of 3, 4, and 5 σ respectively.

In addition to a cut in $P(SN|\frac{S}{N}, log(L))$, the available supernovae template models require that all supernovae $-20 < Age < 70$ (i.e. the template spectra used in the Model Sample span a finite range in supernova age). To mitigate potential edge effects, we include only those supernovae with ages $-14 < Age < 40$ within our final candidates.

Finally, a cut is placed in both $log(L)$ and $\frac{S}{N}$ to avoid catastrophic failures in the algorithm. These are generally due to objects that are not fit well by either galaxy or supernova templates. By inspection, conservative boundaries are set that exclude objects with both $log(L) > 4$ and $\frac{S}{N} < 150$ (see Figure 5). This region is populated by extreme emission line galaxies where the emission lines influence the χ^2-statistic such that a good fit is impossible, and objects for which the spectral calibration failed for one reason or another. These points are not rejected by the $P(SN|\frac{S}{N}, log(L))$ cut because neither training set samples this area of parameter space well.

Together these selection criteria provide a fully automated and probabilistic approach for selection of supernovae from galaxy spectra.

4. SIMULATED SPECTRA AND THE EFFICIENCY OF SUPERNOVA DETECTION

The statistical and systematic properties of our supernova detection and classification technique are determined through a Monte-Carlo simulation using the model sample described in 2 (and Table 1).

4.1. *Efficiency of Supernova Detection in SDSS Spectra*

Host galaxy properties have a large influence on our algorithm's ability to detect the resident supernova. Herein we examine these properties and discuss their impact on

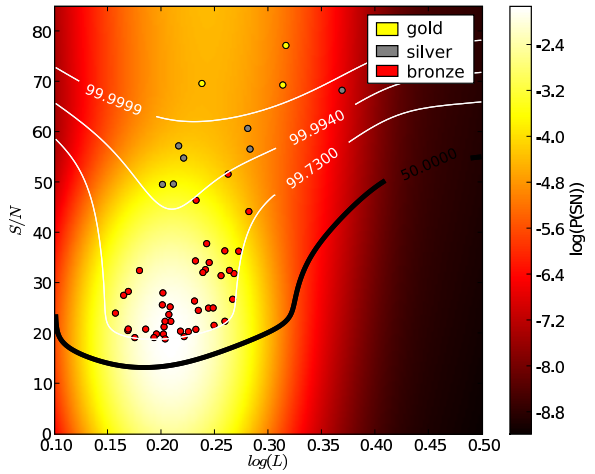

(a) The image shows the probability density of the mixture model trained using the sample with synthetic supernovae added. The contours show the 3,4, and 5σ confidence regions

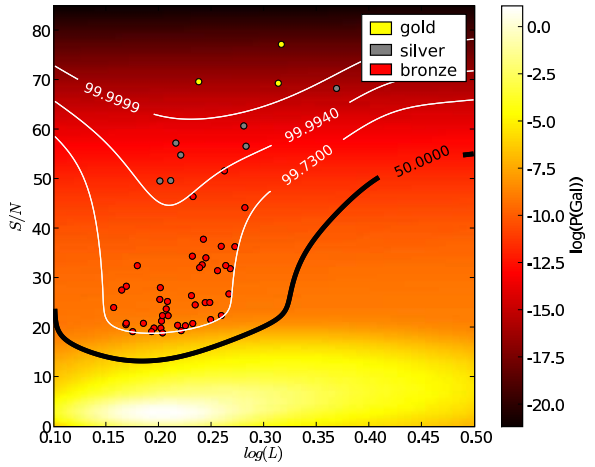

(b) The image shows the probability density of the mixture model trained using the statistical sample. The contours are the same as in a.

FIG. 4.— The training sets for the nonparametric Bayes classifier described in this section. In both panels the color image indicates the probability density of galaxies predicted by the best fit mixture model. The light colors are regions of high probability density and the darker colors are regions of low probability density. The probability density is a proxy for the density of points, so regions of high probability density have more points in the training set. The points are the supernova candidates that satisfy the criterion that $P(SN|\frac{S}{N}, log(L)) > 0.9973$. Red points are bronze candidates, gray points are silver candidates, and yellow points are gold candidates. The thick contour marks the line where a galaxy is equally likely to have a supernova and not have a supernova.

measuring supernova rates. Efficiencies are calculated by applying the selection criteria introduced in the previous section, i.e. we require that the output age is $-14 < age < 40$, $P(SN|\frac{S}{N}, log(L)) \geq 0.9973$, and the region with catastrophic failures is avoided. In the following sections we examine the impact of host galaxy luminosity, redshift, supernova age, host galaxy color and signal-to-noise ratio on the efficiency of the method.

4.2. *Efficiency as Functions of Observables*

Figure 6 shows the efficiency, defined as the ratio of the number of detected supernovae to the number of input supernovae, as a function of r-band absolute magnitude

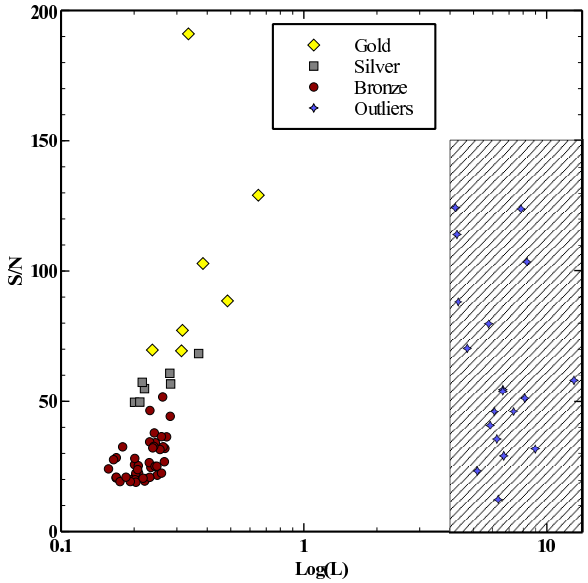

FIG. 5.— The blue circles are sources taken to be supernova candidates. Well separated from this locus is a set of sources (red diamonds) that are clear false positives. These arise due to some spectra have systematic errors from failures in the spectroscopic calibration process, and due to the fact that the fitting templates do not completely span the space in which extreme galaxy emission line spectra reside.

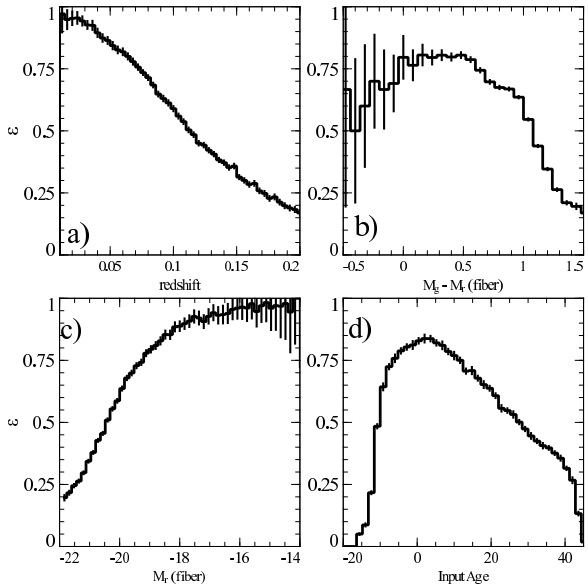

FIG. 6.— Efficiency of the detection algorithm as a function of observables: (a) efficiency as a function of redshift. (b) efficiency as a function of galaxy restframe g-r color. (c) efficiency as a function of absolute k-corrected galaxy fiber magnitude in r. (d) efficiency as a function of input age.

through the fiber, galaxy restframe color, age of the supernova and redshift of the host galaxy.

As shown in Figure 6(a), supernova detection efficiency decreases with redshift (as the signal-to-noise ratio of the underlying spectra will decrease and the sampled galaxy populations will be intrinsically more luminous). The efficiency decreases rapidly beyond a redshift of $z > 0.07$, reaching 50% efficiency at around $z = 0.11$. From the efficiency-signal-to-noise ratio relation shown in Figure 7 we find that this rapid drop in efficiency corresponds

to a median per pixel r-band S/N of 50. This value is calculated by computing the signal-to-noise ratio for each pixel of the spectrum covered by the r-band filter and taking the median value over all pixels. At $z = 0.1$ the fraction of galaxy spectra with $S/N > 50$ is only 3%.

As expected, the efficiency of detection depends on the intrinsic luminosity of the host galaxy; as the luminosity of the host galaxy increases, the efficiency of isolating the supernovae decreases. The intrinsic peak luminosity for type Ia supernovae reaches M_V = -19.5 (Gallagher et al. 2008) with under-luminous supernovae scattering to $M_V \simeq -17.5$. This results in a smooth transition between the regime where the supernovae dominates the spectrum to where the galaxy host dominates. Figure 6(c) demonstrates this effect, showing the decrease in the efficiency of detecting a supernovae remaining at about 75% to $M_{fiber_r} = 18$ and then dropping quickly to 30% at $M_{fiber\_r} = -20$ (at which point the galaxy is contributing about 50% more light than the peak brightness supernova).

One might expect the detection of supernovae to be independent of the color of the galaxy as there are spectral features distributed throughout the optical spectral range. Figure 6(b) shows, however, a color dependence in the detection efficiency such that supernova detection in red galaxies has a lower efficiency than for blue galaxies. This is due to the correlation between luminosity and intrinsic galaxy color. If the Model Sample is binned in absolute magnitude and the efficiencies replotted as a function of restframe color, the efficiency curve is flat but the normalization of that curve decreases with luminosity.

We also consider the efficiency as a function of supernova age in Figure 6(d). The integral of this histogram is the control time, τ, which dictates the temporal window over which a supernova is detectable. As shown in Figure 6(d), the impact on efficiency occurs at early and late times when the supernova luminosity is closest to a minimum in our templates. For ages $-10 < days < +20$, the efficiency of supernova detection remains above 50%.

4.3. *Signal to Noise Ratio*

Based on the results described above, the most important efficiency indicator for the rate of supernova detection is that of S/N of the measured spectrum. The signal-to-noise ratio incorporates all of the dependencies on galaxy and supernova properties in the efficiency calculation. In each of the previous results, the drop in efficiency was related to a decrease in supernova signal-to-noise ratio (either absolute or relative to the galaxy luminosity). We therefore approximate the signal-to-noise ratio of the measured spectrum (including the supernova) as the median of the signal-to-noise ratios of the spectral bins in the r passband. Figure 7 shows this efficiency as a function of median r-band S/N. As expected the efficiency decreases with lower signal-to-noise ratios, but remains above 50% down to $S/N = 23$ (which represents 70% of galaxies in the statistical sample).

5. APPLICATION TO SDSS

The algorithm described in §3 and the criteria from §3.1 were applied to the SDSS spectra from the DR5 statistical sample. To quantify the effectiveness of these techniques we define subsamples of supernovae

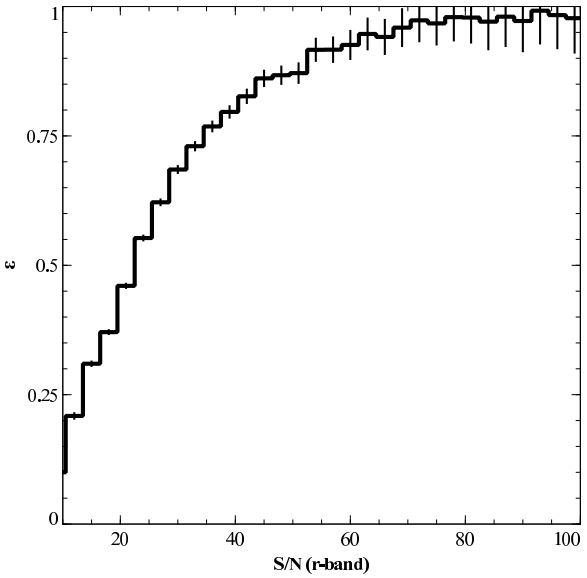

FIG. 7.— Efficiency as a function of signal-to-noise ratio of the measured (galaxy + supernova) spectrum in the r-band

as a function of their classification probability. These supernovae, gold ($P(SN|\frac{S}{N}, log(L))$ >0.99999943), silver ($P(SN|\frac{S}{N}, log(L))$ >0.999937), and bronze ($P(SN|\frac{S}{N}, log(L))$ >0.9973), are shown in Figure 5. Visual inspection of these supernova candidates shows that: gold candidates have many (greater than four) spectral features in the residual fit that are coincident with the best fit template, silver candidates have at least three features that match the template and exceed the noise in the spectrum, and bronze class sources have at least three well fit features, but with per pixel signal at the level of the per pixel error. Figure 8 shows examples of these three classes. The bronze candidate spectra were smoothed with a 5 bin tophat filter to show more clearly how the low frequency signal matches the template spectra.

For reference, we show the distribution in color and redshift for the statistical and candidate samples. Figure 9(a) shows that the color distribution is similar for both populations. The redshift distributions, however, are quite different. As seen in Figure 9(b) the candidate supernova population has a much flatter distribution than the parent population. This is likely due simply to the increased efficiency of finding supernovae in nearby galaxies. Note that the redshift distribution is truncated at $z = 0.2$. In Figure 10 we show the distribution of measured ages from peak for the candidate supernovae. Obviously the number of candidates is not large enough to fully sample the range of templates, but we do recover supernovae over essentially the entire window of possible ages.

5.1. *Direct Confirmation of supernovae*

To validate the accuracy of the detection algorithm we undertake a number of tests on the derived spectra. The first of these is a comparison of the fiber magnitudes measured from the photometry with synthetic magnitudes calculated from the observed spectra. The fiber magnitudes are computed by placing a 3" diameter aperture at the centroid of the seeing convolved object. The

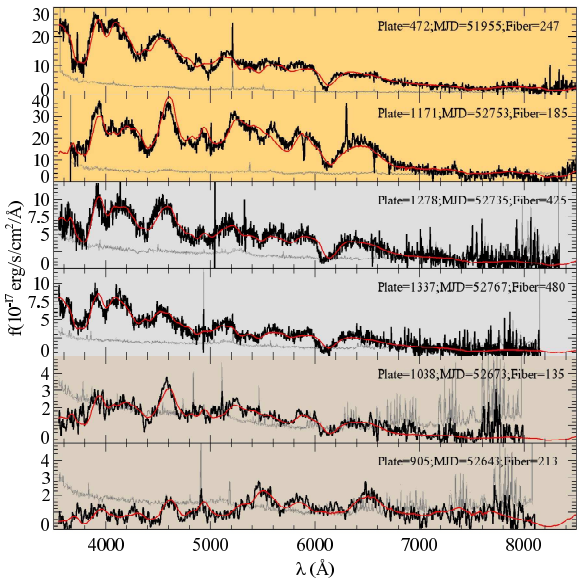

FIG. 8.— Six examples of supernova candidates selected using the algorithm presented in this paper. The top two panes are for the "gold" sample, the middle two panes are for the "silver" sample, and the bottom two panes are for the "bronze" sample. The residual after the galaxy component is subtracted is shown in black. The best fit template is plotted in red and the rms uncertainty as reported by the pipeline is in gray. The plate, mjd, and fiber are provided in the upper right of each pane.

synthetic magnitudes are calculated by integrating the product of the filter transmission curves and the observed spectrum. We obtain the fiber and synthetic magnitudes in the r-band for all objects in the full sample. In the absence of transient events one would expect the two values to be equivalent. Figure 11 shows the difference between the fiber and synthetic magnitudes as a function of fiber magnitude (for the statistical sample). The supernova candidates are plotted as circles. Yellow circles are gold candidates, gray circles are silver candidates and red circles are bronze candidates.

Of the 52 supernova candidates, all show a brightening in the synthetic magnitude as compared to the fiber magnitude. This is consistent with additional flux contribution from transient sources.

Of the 52 supernovae used in the rate calculation, four were observed spectroscopically on more than one occasion. All four cases show a brightening in the supernova containing spectrum. In all four cases the difference of the two epochs show similar feature to the residual spectrum from the fitting algorithm. A typical example, SDSS J124733.40+000557.1, was observed on MJD 51660 and 268 days later on MJD 51928. The supernova was detected in the later epoch with an estimated age of 27 days after maximum. This candidate was detected as a member of the bronze sample with $P(SN|\frac{S}{N}, log(L)) = 0.9986$. Given these repeat observations we subtract the two spectra (which removes the uncertainty in the modeling of the host galaxy spectrum) and show the two spectra together in the top pane of Figure 12. In the middle pane we plot the difference of the flux in the two epochs with the best fit template spectrum scaled as calculated by the algorithm. Clearly the difference spectrum and the template agree. Finally, we plot the ratio of the difference spectrum to the supernova signal from epoch 2. At shorter wavelengths it appears

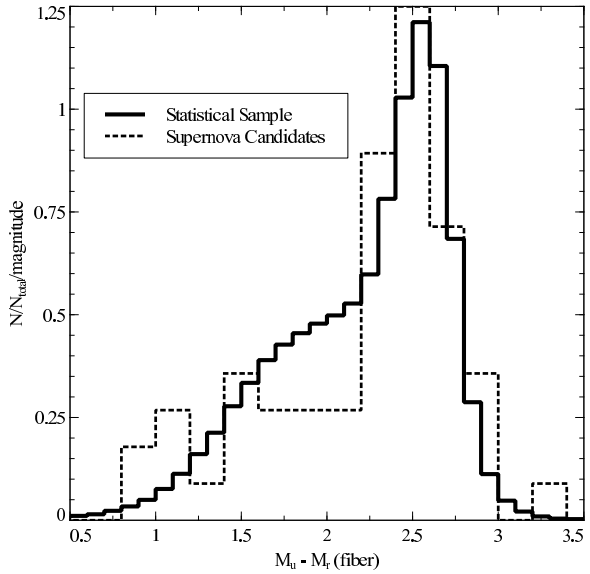

(a) Comparison of fiber $u-r$ color distribution for the statistical sample (solid) and supernovae (dotted). The magnitudes are absolute K-corrected fiber magnitudes.

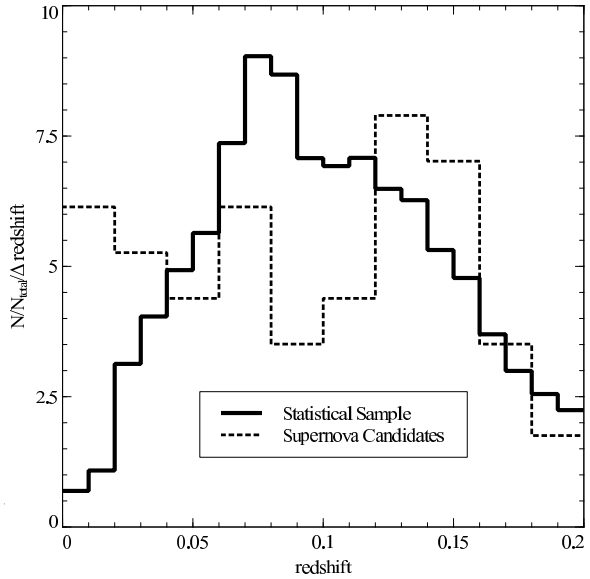

(b) Comparison of redshift distribution for the statistical sample (solid) and supernovae (dotted).

FIG. 9.— Comparison of supernova candidate distributions to the distribution of the statistical sample.

that the fitting algorithm is under-subtracting the galaxy contribution. In this example the under-subtraction is $< 5\%$ of the total spectrum flux. This shows that the fitting algorithm does a very good job in this case of superimposed galaxy and supernova signal.

These two pieces of evidence, the brightening of objects in the spectrum relative to the photometry, and multi-epoch spectroscopic observations showing supernova signatures indicate strongly that the algorithm is selecting real supernova signatures.

6. TYPE IA LUMINOSITY WEIGHTED SUPERNOVA RATE

Based on the efficiency calculations in §4 and the supernovae identified in the statistical sample we calculate the supernovae rate for galaxies at a mean redshift of

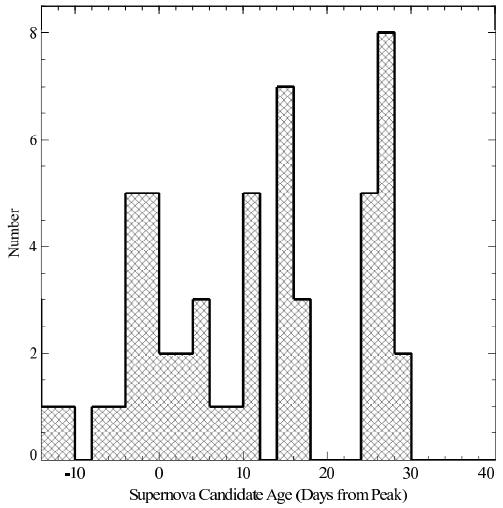

FIG. 10.— Distribution of measured rest frame ages for the 52 SN candidates used in the rate calculation.

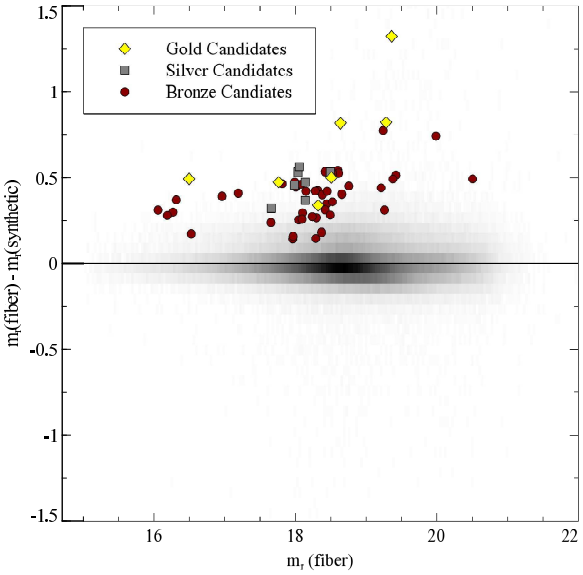

FIG. 11.— For all detected supernovae, we plot the difference in the r-band fiber and synthetic magnitudes against the r-band fiber magnitude. Fiber magnitudes are aperture magnitudes calculated from the photometry. Synthetic magnitudes are calculated by integrating the observed spectrum convolved with fiducial filter curves. The density plot is the entire SDSS DR5 spectroscopic sample. Gold candidates are plotted in yellow (diamonds), silver in gray (squares), and bronze in red (circles). In general, the spectra are brighter than their photometric counterparts, suggesting an extra flux contribution.

$z = 0.1$. The luminosity weighted supernova rate (r_L) is traditionally defined as:

$$\langle N_{SN} \rangle = r_L \times S, \tag{5}$$

where $\langle N_{SN} \rangle$ is the expected number of type Ia supernovae and S is the sum of the probability of detecting a supernova in a given galaxy, weighted by the luminosity in the B-band, in units of $L_\odot$,

$$S = \sum_i^{N_{gal}} L_i \epsilon_i \tau_i. \tag{6}$$

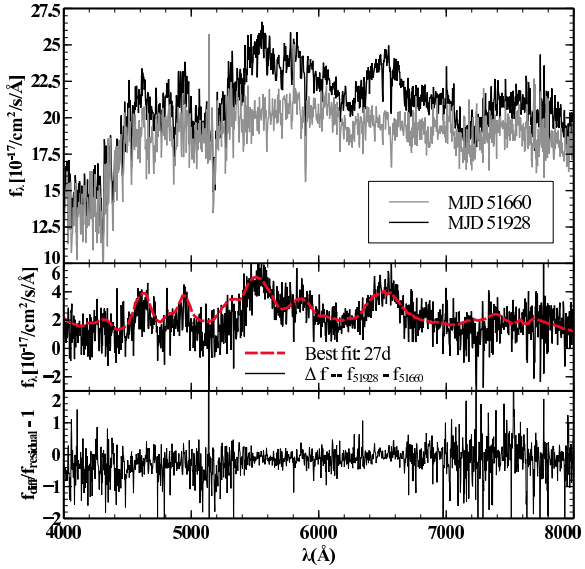

FIG. 12.— An example of an object with two epochs in spectroscopy of object SDSS j124733.40+000557.1. In the upper panel Epoch 2 (black) with the SN contribution is obviously brighter than the spectrum taken at the earlier Epoch 1 (gray). The middle panel shows the comparison of the difference of Epoch 2 and Epoch 1 (black) to the best fit template as chosen by the SN selection algorithm (red dashed). The best fit template is age 27 days. The bottom panel is the ratio of the difference spectrum to the galaxy subtracted supernova.

The sum runs over all galaxies in the statistical sample. L_i is the rest frame B-band luminosity in units of $L_\odot$ and τ_i is the time period we are sensitive to identify supernova. The efficiency ϵ is a function of redshift, apparent magnitude, luminosity, galaxy type, seeing, and other observables. As in Dilday et al. (2008), we avoid the complexity involved in modeling the efficiency as a joint distribution of all characteristics by using the efficiency as a function of signal-to-noise ratio. The control time τ is then defined as:

$$\tau = \sum_{z=0.0}^{z=0.2} \epsilon_z(z) * \int_{t_1}^{t_2} \epsilon_t(t,z) dt \tag{7}$$

where t is the age of the supernova with peak brightness occurring at $t = 0$ and $\epsilon(t)$ is the efficiency as a function of supernova age. We use the window $-14 \leq age \leq 40$ as this is the interval over which $\epsilon(t)$ was evaluated. We use a redshift averaged value of τ using the redshift distribution for the statistical sample (see Figure 9(b)) to obtain the typical detection window for the survey as a whole. We evaluate this integral to obtain the fraction of a year over which the algorithm is sensitive to detecting type Ia supernovae. For this survey $\tau = 0.1$ yr.

We calculate the luminosity weight in two ways. First, we consider only the contribution of flux from within the fiber. This takes a local view of the luminosity weighting by allowing for only stellar light encompassed by the fiber. A second approach is to rescale the luminosity by the covering factor of the fiber relative to the galaxy total flux. This covering factor is calculated as:

$$cf = 10^{(M_{model} - M_{fiber})/2.5}. \tag{8}$$

In the above equation, the k-corrected, absolute magnitudes may be in any band but, as the galaxy sample is

r-band selected, we use the r-band to calculate the covering factor. In some cases, however, the fiber magnitude is brighter than the model magnitude due to blending of overlapping galaxies. In order to avoid these issues, we discard galaxies where $M_{fiber} < M_{model}$. This situation is encountered in 0.5% of the galaxy sample. This results in 360,698 galaxies used in the covering factor method of calculating the rate.

In general, using the flux through the fiber is preferable since there is no dependence on photometric model fitting. The model fitting could potentially introduce a bias in the covering factor as a function of galaxy morphology. For this reason, we use the fiber-based B-band luminosity weighted rate for comparison to other published values and in reporting the rate as a function of galaxy color.

We further subdivide the sample into red and blue subsets using a color cut of $M_u - M_r = 2.2$ to estimate the supernova rate as a function of galaxy spectral type. Strateva et al. (2001) suggest that a value of 2.2 gives optimal separation between early and late type galaxies. We use this value to separate the statistical sample into an early (red) and late (blue) galaxy sample. In this case these values have been calculated using the measured fiber flux in order to maximize the size of the supernova sample.

Solving Equation 5 for r_L, and applying the calculated values of S and N_{SN}, we obtain a value of r_L given a given value from Equation 4. In order to get the best estimate of the rate given the variance inherent in the sample we select many values of the cutoff: $0.9973 \leq P(SN|\frac{S}{N}, Log(L)) \leq 1.0$. The lower limit corresponds to a 3σ and is the cut used in producing the plots presented in Figures 6 and 7. In practice, new efficiency curves are calculated for each selected value of the probability cut. We calculate the rate for 100 different selections of the selection cutoff. We then find the inverse variance weighted mean of the rates. This weighting was chosen with the expectation that more stringent cuts would produce less candidates but be less likely to include false positives. If there is no contamination from interlopers, even at the 3σ level, the inverse variance weighting should have no impact on the mean. See §6.1.4 for discussion of systematic error contribution of varying the threshold. The weighted mean yields $r_L = 0.472 \pm 0.08 h_{70}^2 SNu$ which assumes that the supernova rate is proportional to the rest frame B-band galaxy luminosity. The statistical error is the central 68.3% Poisson confidence interval assuming the median number of supernova candidates (45) for the 100 data points. The supernova rate values and details of the errors are summarized in Table 2. Note that the total number of supernovae listed in the table in column 6 differs from that listed in Table 1. This is due solely to the fact that the $-14 < Age(Days) < 40$ age cut was not applied to the candidates selected from the Statistical Sample. The supernova rates for the red and blue samples are $r_L(red) = 0.379 \pm 0.08$ and $r_L(blue) = 0.394 \pm 0.12$, respectively. As seen in other samples, the luminosity weighted rate from blue galaxies is higher than that from red galaxies, however they are consistent within errors.

6.1. *Systematic Errors in Supernovae Rates*

We consider potential systematics in our derived values of r_L.

6.1.1. *Color corrections to a B-band luminosity*

We compare the derived B luminosity for the host galaxies using two relations for color transformations between the SDSS and Johnson B passbands. These color corrections are taken from Lupton (2005)[11] and Jester et al. (2005). Specifically the corrections are:

$$B = g + 0.33 * (g - r) + 0.20 Jesteretal.(2005) \quad (9)$$

$$B = g + 0.3130 * (g - r) + 0.2271 \quad (10)$$

The difference between these solutions amounts to $\pm 3\%$ in the derived luminosities.

6.1.2. *Type Ib/c Contamination*

Since we use only type Ia templates for candidate selection, it is possible that type Ib/c supernovae could be a source of false positives. To test how sensitive this algorithm is to type Ib/c interlopers, we simulate perfect galaxy subtraction by fitting our set of type Ia templates directly to type Ib/c templates (Levan et al. (2005)) at various signal to noise levels. We can then plot the results of the fit directly on in the same space as that used for candidate selection. Figure 13 shows where the type Ib/c spectra fall on the $Log(L) - -\frac{S}{N}$ space. Many are excluded by the 3σ confidence threshold (dashed line). Those that do pass are well separated from the candidates in our sample. If we had candidates in the region of the discriminate space occupied by the type Ib/c spectra, we would need to account for the possibility of contamination. The locus of our sample is very well separated from that of the type Ib/c candidates, our sample shows no evidence of contamination by type Ib/c supernovae.

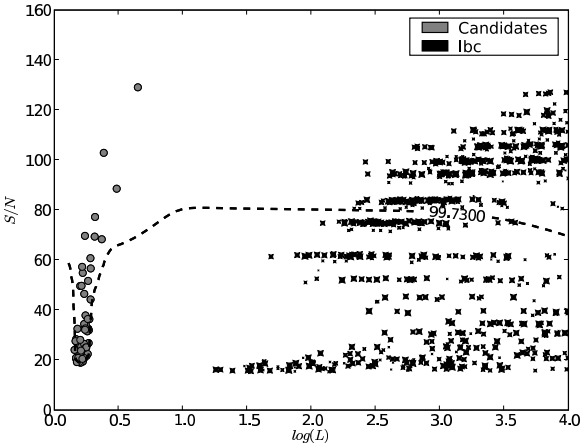

FIG. 13.— Type Ia candidates (circles) plotted with the results of fitting type Ib/c spectra with type Ia templates (stars). The size of the point indicates the age of the type Ib/c candidate. The dotted line is the 3σ threshold applied when selecting candidates. Many of the candidates are ruled out by the threshold.

[11] http://www.sdss.org/dr7/algorithms/sdssUBVRITransform.htmlk#Lupton2005

6.1.3. *Efficiency Uncertainty*

The efficiency histogram has an intrinsic uncertainty due to shot noise (based on the number of galaxies in each bin). Propagating Poisson errors on the signal-to-noise ratio efficiency shows an uncertainty of not more than 2% in the rate calculation when 1σ errors are considered. We adopt a value of 2% for the contribution of uncertainty of efficiency.

6.1.4. *Uncertainty in Threshold Cut*

The value of Equation 4 gives a good discriminant for distinguishing supernova candidates, but the choice of the cutoff value influences the calculated value of the rate. To get a handle on how much this affects the rate value we calculate rates using 100 different choices for the cutoff. We then calculate the inverse variance weighted mean of the rate give the 100 data points. We then quantify the scatter by calculating the standard deviation of the sample greater than the mean and the standard deviation of the sample less than the mean. This analysis gives a positive scatter of 9.5% and a negative scatter of 7.5%. The fact that the scatter to higher values of the rate is larger than to lower values suggests that there is some contamination from interlopers, but that when several values of the cutoff are taken, the effect on the measured rate is small.

Adding these contributions in quadrature this estimate of the systematic error corresponds to $^{+10.2\%}_{-8.3\%}$.

7. COMPARISON TO MODELS

Many type Ia supernova rate (SNR_{Ia}) measures have recently appeared in the literature, often at higher redshift than previously sampled. Measures at high redshift ($z > 1$) are generally given in units of the comoving volumetric element. In order to directly compare the rate derived in this paper with those in the literature, we convert luminosity weighted rates to volumetric rates using the B-band luminosity density. As in Horesh et al. (2008) we use the redshift dependent form $j_B(z) = (1.03 + 1.76 \times z) \times 10^8 L_{\odot} Mpc^{-3}$ from Botticella et al. (2008). Table 3 is a collation of SNR_{Ia} from the literature. We have ordered them in mean redshift to facilitate comparison of values at similar distances.

The cosmic supernova rate is notoriously difficult to measure as the number of events is usually small, the systematics are numerous and hard to correct for, and even the data on a per object basis can be less than ideal because of their transient nature. All these factors contribute to large errors, which make differentiation between different predictions difficult.

Two formulations of the analytic SNR_{Ia} are typically used. The delay time distribution (DTD) formulation can be expressed using the the notation of Greggio (2005), the SNR_{Ia}(t) is defined:

$$SNR_{Ia}(t) = k_{\alpha} \int_{\tau_i}^{min(t,\tau_x)} A_{Ia}(t-\tau)\dot{\rho}(t-\tau) f_{Ia}(\tau) d\tau \tag{11}$$

where k_{α} is the normalization of the initial mass function (taken to be 2.83 for the Salpeter IMF), A_{Ia} is the efficiency of the progenitor channel, $\dot{\rho}$ is the cosmic star formation rate, and f_{Ia} is the distribution of times between birth and explosion also denoted DTD_{Ia}. A_{Ia} is typically taken to be constant with time, but in general can evolve with the stellar population.

The "A+B" model formalized in Sullivan et al. (2006) scales a tardy component and a prompt component based on the integrated stellar mass build-up and instantaneous star formation rate, respectively. Using the notation of Hopkins & Beacom (2006),

$$SNR_{Ia} = A\rho_*(t) + B\dot{\rho_*}(t). \tag{12}$$

Both the DTD and "A+B" methods can have short and long timescale contributions to the total SNR_{Ia} at any given time, but the DTD formulation allows much more latitude in the spectrum of the delay times. Hopkins & Beacom (2006) modified the "A+B" model by allowing for a delta function delay time in the prompt component effectively setting a characteristic delay time. They found that they could set the tardy component to zero, yielding:

$$SNR_{Ia} = B\dot{\rho}(t-\tau) \tag{13}$$

where τ is the delay time and is $3Gyr$.

Most DTD models rely on white dwarf binary systems as progenitors of type Ia supernovae. However, it is not yet clear what the companion star is in these binary systems (Branch et al. 1995; Parthasarathy et al. 2007). Many groups have attempted to constrain DTDs (see Valiante et al. 2009; Ruiter et al. 2009; Totani et al. 2008; Hachisu et al. 2008; Greggio et al. 2008, and others). Recent measurements and models of the type Ia DTD imply a featureless power law. The two main channels for type Ia supernova progenitors are the single degenerate (SD; white dwarf with non-degenerate star (Whelan & Iben 1973)) and double degenerate (DD; white dwarf binary(Iben & Tutukov 1984)) scenarios. Models of the DD path show that a featureless power law is in agreement with the predicted DTD from the DD contribution (Totani et al. (2008) and references therein). Recently, it was shown that the SD path can produce a power law DTD when both white dwarf + main sequence and white dwarf + red giant systems are considered (Hachisu et al. 2008). Direct measurements also support power law DTDs for type Ia supernovae (Totani et al. 2008; Pritchet et al. 2008). The power law DTD is attractive because of it's simplicity and the fact that it has contribution from both prompt and tardy components.

There is much discussion about which model for the evolution of the cosmic type Ia supernova rate is the most appropriate, but even for power law DTD models exponent of the power law α is under debate. Theoretical values seem to point to a steep power law $\alpha \simeq -1.0$ from both SD and DD channels (Hachisu et al. 2008; Yungelson & Livio 2000; Greggio 2005). The value as measured from data in (Totani et al. 2008) agrees well with $\alpha = -1.0$, although Pritchet et al. (2008) find a shallower power law with $\alpha \simeq -0.5$.

Changing from cosmic time to redshift and substituting a power law for the DTD model, we produce the following formula:

$$SNR_{Ia}(z) = k_a \int_{0.3}^{t(z)} A_{Ia}\dot{\rho}_*(t(z)-\tau)\tau^{\alpha} d\tau \tag{14}$$

where $t(z)$ is the cosmic time at redshift z, $\dot{\rho}_*$ is the cosmic star formation rate, t is the delay time and α is the slope of the power law. The product of $k_a A_{Ia}$ is the constant for which we fit. It should be noted that we are not attempting to pin down any physical constants to higher precision than is already reported in the literature. The error bars used are statistical in all cases. No attempt has been made to cull the data of unreliable data points as the model fitting is intended to be illustrative rather than diagnostic. Figure 14 shows the data from the literature fit using the above models with $\alpha = -1$ (dashed line). This model, supported by theory and data, over predicts the rate at both low and high redshift, except for the point at $z = 1.2$ from Poznanski et al. (2007), who question the sharp decline in SNR_{Ia} after $z = 1.5$.

The A+B model appears to be too flat to account for both the rise in rate from $z = 0$ to $z \simeq 1.0$ and the decline after $z = 1.5$. Since a large part of the best fit A+B model is contributed by the prompt ($\dot{\rho}_*$) component which does not peak until $z \simeq 2$, it is not surprising that it continues to rise at high redshift. As mentioned above, Hopkins & Beacom (2006) noticed that a modified A+B ($SNR = A\rho_*(t) + B\dot{\rho}_*(\tau - \tau_{Ia})$; Scannapieco & Bildsten (2005)) type model with $A = 0$ and a delta function delay time distribution do just as well in describing the observed downturn at $z \simeq 1$. Figure 14 shows the best fit Scannapieco & Bildsten (2005) model with fixed delay time $\tau_{Ia} = 3Gyr$. In this scenario, the accrued stellar mass contributes nothing to the cosmic SNR. Instead, type Ia supernovae arise after a fixed waiting period after a star formation event. This model is certainly an over simplification as a broad distribution of assembly times surely exist for both the SD and DD scenarios.

The result from this work is higher than other measurements at low redshift, but is within the error bars of all of them. A possible explanation of the higher measurement is that systematic effects tend to drive efficiency down. This leads to lower predicted rate measurements if these effects are not taken into account. This argues for a greater level of correction in the measurement from this paper as compared to others for $z < 0.3$. Despite being higher than other measurements, our value is still lower than two of the three models explored in this paper. The model that is closest to the low redshift values is that of the constant delta function delay time model.

Current models for the DTD of type Ia supernovae show good agreement with the data despite DTDs as different as power law and delta functions. The ability for observed supernova rates to distinguish between these models will depend on reliable SNR measurements at $z = 2.0$.

8. CONCLUSIONS

From a sample of 362,431 galaxies we detect 57 (52 of which meet all criterion for calculating the supernova rate) type Ia supernovae within SDSS spectroscopic observations by modeling and subtracting the host galaxy component. Extensive Monte Carlo simulations of the efficiencies and systematics present in these samples are used to determine a type Ia supernova rate of 0.472 $h_{70}^2 SNu$ at a mean redshift of $z = 0.1$. The measurement published here is higher than others at $z < 0.2$, but agrees within 1 sigma statistical errors with the other published values. It is interesting to note that the bias for this study is strongly toward finding supernovae in the central parts of galaxies. This is opposite to the bias of difference imaging type surveys which are slightly biased away from finding supernovae in the central parts of galaxies due to the brightness of the cores as well as dust extinction.

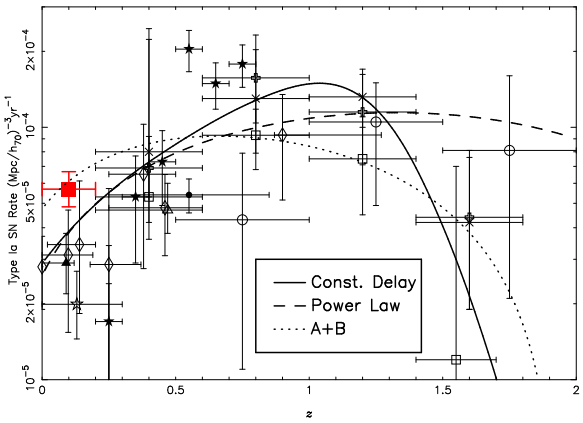

FIG. 14.— Latest volumetric supernova rates with three models: a constant delay time of 3Gyr, an A+B model and a power law model with $\alpha = -1.0$. The value from this work with error bars is plotted in red.

Despite our measurement being slightly higher than others at similar redshift, there is still a significant rise in the type Ia rate from our value at $z = 0.1$ to redshift of unity. One possible explanation for this trend is that we were able to incorporate many contributors to the efficiency calculation including realistic estimates of host extinction and peak supernova luminosity. Almost any modeled physical effect will tend to drive efficiency down resulting in higher recovered rate measurements. This study is based on one of the largest samples of supernovae in the local universe. Subdividing the galaxy population into red and blue components, we find no evidence for a difference in supernova rate as a function of host galaxy rest frame color within errors.

The success of this study demonstrates that spectroscopic surveys can be used to identify and classify supernova and supernova rates in the local and distant universe in a serendipitous manner. The next generation of wide field spectroscopic surveys such as BOSS (Schlegel et al. 2009) we will have the potential to detect thousands of supernova in a much larger volume than that sampled by the SDSS spectroscopic sample.

9. ACKNOWLEDGMENTS

Funding for the SDSS and SDSS-II has been provided by the Alfred P. Sloan Foundation, the Participating Institutions, the National Science Foundation, the U.S. Department of Energy, the National Aeronautics and Space Administration, the Japanese Monbukagakusho, the Max Planck Society, and the Higher Education Funding Council for England. The SDSS Web Site is http://www.sdss.org/.

The SDSS is managed by the Astrophysical Research Consortium for the Participating Institutions. The Participating Institutions are the American Museum of Natural History, Astrophysical Institute Potsdam, University of Basel, University of Cambridge, Case Western Reserve University, University of Chicago, Drexel University, Fermilab, the Institute for Advanced Study, the

Japan Participation Group, Johns Hopkins University, the Joint Institute for Nuclear Astrophysics, the Kavli Institute for Particle Astrophysics and Cosmology, the Korean Scientist Group, the Chinese Academy of Sciences (LAMOST), Los Alamos National Laboratory, the Max-Planck-Institute for Astronomy (MPIA), the Max-Planck-Institute for Astrophysics (MPA), New Mexico State University, Ohio State University, University of Pittsburgh, University of Portsmouth, Princeton University, the United States Naval Observatory, and the University of Washington.

REFERENCES

Adelman-McCarthy, J. K., et al. 2007, ApJS, 172, 634
Alard, C., & Lupton, R. H. 1998, ApJ, 503, 325
Barris, B. J., & Tonry, J. L. 2006, ApJ, 637, 427
Blanc, G., et al. 2004, A&A, 423, 881
Botticella, M. T., Riello, M., Cappellaro, E., Benetti, S., Altavilla, G., Pastorello, A., Turatto, M., Greggio, L., Patat, F., Valenti, S., Zampieri, L., Harutyunyan, A., Pignata, G., & Taubenberger, S. 2008, A&A, 479, 49
Branch, D., Buta, R., Falk, S. W., McCall, M. L., Uomoto, A., Wheeler, J. C., Wills, B. J., & Sutherland, P. G. 1982, ApJ, 252, L61
Branch, D., Livio, M., Yungelson, L. R., Boffi, F. R., & Baron, E. 1995, PASP, 107, 1019
Bruzual, G., & Charlot, S. 2003, MNRAS, 344, 1000
Cappellaro, E., Evans, R., & Turatto, M. 1999, A&A, 351, 459
Cardelli, J. A., Clayton, G. C., & Mathis, J. S. 1989, ApJ, 345, 245
Connolly, A. J., Szalay, A. S., Bershady, M. A., Kinney, A. L., & Calzetti, D. 1995, AJ, 110, 1071
Dahlen, T., Strolger, L.-G., & Riess, A. G. 2008, ApJ, 681, 462
Dahlen, T., Strolger, L.-G., Riess, A. G., Mobasher, B., Chary, R.-R., Conselice, C. J., Ferguson, H. C., Fruchter, A. S., Giavalisco, M., Livio, M., Madau, P., Panagia, N., & Tonry, J. L. 2004, ApJ, 613, 189
Dilday, B., et al. 2008, ApJ, 682, 262
Folkes, S. R., Lahav, O., & Maddox, S. J. 1996, MNRAS, 283, 651
Frieman, J. A. et al. 2008, AJ, 135, 338
Fukugita, M., Ichikawa, T., Gunn, J. E., Doi, M., Shimasaku, K., & Schneider, D. P. 1996, AJ, 111, 1748
Gal-Yam, A., Maoz, D., & Sharon, K. 2002, MNRAS, 332, 37
Gallagher, J. S., Garnavich, P. M., Caldwell, N., Kirshner, R. P., Jha, S. W., Li, W., Ganeshalingam, M., & Filippenko, A. V. 2008, ApJ, 685, 752
Goldhaber, G., et al. 2001, ApJ, 558, 359
Greggio, L. 2005, A&A, 441, 1055
Greggio, L., Renzini, A., & Daddi, E. 2008, MNRAS, 388, 829
Gunn, J. E., et al. 1998, AJ, 116, 3040
Gunn, J. E., et al. 2006, AJ, 131, 2332
Hachisu, I., Kato, M., & Nomoto, K. 2008, ApJ, 683, L127
Hamuy, M., et al. 2006, PASP, 118, 2
Hardin, D., et al. 2000, A&A, 362, 419
Hicken, M., et al. 2009, ApJ, 700, 331
Hogg, D. W., Finkbeiner, D. P., Schlegel, D. J., & Gunn, J. E. 2001, AJ, 122, 2129
Hopkins, A. M., & Beacom, J. F. 2006, ApJ, 651, 142
Horesh, A., Poznanski, D., Ofek, E. O., & Maoz, D. 2008, MNRAS, 389, 1871
Iben, Jr., I., & Tutukov, A. V. 1984, ApJS, 54, 335
Ivezić, Ž., et al. 2004, Astronomische Nachrichten, 325, 583
Jester, S., et al. 2005, AJ, 130, 873
Kuznetsova, N., et al. 2008, ApJ, 673, 981
Levan, A., et al. 2005, ApJ, 624, 880
Madgwick, D. S., Hewett, P. C., Mortlock, D. J., & Wang, L. 2003, ApJ, 599, L33
Mannucci, F., Della Valle, M., & Panagia, N. 2006, MNRAS, 370, 773
Miknaitis, G., et al. 2007, ApJ, 666, 674
Moore, A. 1998, Neural Information Systems Processing
Neill, J. D., et al. 2006, AJ, 132, 1126
Nugent, P., Baron, E., Branch, D., Fisher, A., & Hauschildt, P. H. 1997, ApJ, 485, 812
O'Donnell, J. E. 1994, ApJ, 422, 158
Padmanabhan, N., et al. 2008, ApJ, 674, 1217
Pain, R., et al. 2002, ApJ, 577, 120
Pain, R., et al. 1996, ApJ, 473, 356
Parthasarathy, M., Branch, D., Jeffery, D. J., & Baron, E. 2007, New Astronomy Review, 51, 524
Perlmutter, S., et al. 1999, ApJ, 517, 565
Pier, J. R., Munn, J. A., Hindsley, R. B., Hennessy, G. S., Kent, S. M., Lupton, R. H., & Ivezić, Ž. 2003, AJ, 125, 1559
Poznanski, D., et al. 2007, MNRAS, 382, 1169
Pritchet, C. J., & For The Snls Collaboration. 2005, in Astronomical Society of the Pacific Conference Series, Vol. 339, Observing Dark Energy, ed. S. C. Wolff & T. R. Lauer, 60–+
Pritchet, C. J., Howell, D. A., & Sullivan, M. 2008, ApJ, 683, L25
Richards, G. T., et al. 2004, ApJS, 155, 257
Ruiter, A. J., Belczynski, K., & Fryer, C. 2009, ApJ, 699, 2026
Scannapieco, E., & Bildsten, L. 2005, ApJ, 629, L85
Schlegel, D., White, M., & Eisenstein, D. 2009, ArXiv e-prints
Schlegel, D. J., Finkbeiner, D. P., & Davis, M. 1998, ApJ, 500, 525
Schmidt, B. P., et al. 1998, ApJ, 507, 46
Sivanandam, S., Zabludoff, A. I., Zaritsky, D., Gonzalez, A. H., & Kelson, D. D. 2009, ApJ, 691, 1787
Smith, J. A., et al. 2002, AJ, 123, 2121
Stoughton, C., et al. 2002, AJ, 123, 485
Strateva, I., et al. 2001, AJ, 122, 1861
Strauss, M. A., et al. 2002, AJ, 124, 1810
Sullivan, M., et al. 2006, ApJ, 648, 868
Tonry, J. L., et al. 2003, ApJ, 594, 1
Totani, T., Morokuma, T., Oda, T., Doi, M., & Yasuda, N. 2008, PASJ, 60, 1327
Tucker, D. L., et al. 2006, Astronomische Nachrichten, 327, 821
Valiante, R., Matteucci, F., Recchi, S., & Calura, F. 2009, New Astronomy, 14, 638
Whelan, J., & Iben, I. J. 1973, ApJ, 186, 1007
Wood-Vasey, W. M., et al. 2004, New Astronomy Review, 48, 637
Yip, C. W., Connolly, A. J., Szalay, A. S., Budavári, T., SubbaRao, M., Frieman, J. A., Nichol, R. C., Hopkins, A. M., York, D. G., Okamura, S., Brinkmann, J., Csabai, I., Thakar, A. R., Fukugita, M., & Ivezić, Ž. 2004a, AJ, 128, 585
Yip, C. W., Connolly, A. J., Vanden Berk, D. E., Ma, Z., Frieman, J. A., SubbaRao, M., Szalay, A. S., Richards, G. T., Hall, P. B., Schneider, D. P., Hopkins, A. M., Trump, J., & Brinkmann, J. 2004b, AJ, 128, 2603
York, D. G., et al. 2000, AJ, 120, 1579
Yungelson, L. R., & Livio, M. 2000, ApJ, 528, 108

Sample	Number of Spectra	N_{SNe}	Notes
Statistical Sample	362,431	52	G=7,S=7,B=43
Model Sample	234638	N/A	

TABLE 1

The samples used in this paper. The first column gives the name of the sample as it is used in the text. Column 2 gives the sample size. In Column 3 we report the number of supernova candidates in the sample. This is the total number of candidates. The number listed here includes all selection criteria listed in §3.1. This number increases to 57 if no age cut is applied. Any notes are given in Column 4. In particular, the number of gold (G), silver (S), and bronze (B) candidates are noted. For a description of how the gold, silver and bronze candidates are defined, see §3.1.

Method	Value (SNu)	Sys. Error (SNu)	Stat. Error (SNu)	$\overline{N_{SN}}$	N_{SN}
Covering Factor	0.454	$^{+0.046}_{-0.038}$	$^{+0.079}_{-0.068}$	44	51
Fiber	0.472	$^{+0.048}_{-0.039}$	$^{+0.081}_{-0.070}$	45	52
Red	0.379	$^{+0.039}_{-0.031}$	$^{+0.080}_{-0.067}$	32	36
Blue	0.394	$^{+0.040}_{-0.033}$	$^{+0.142}_{-0.108}$	13	16

TABLE 2

The results from applying the algorithm to the SDSS Statistical Sample. Column 1 describes the method used, the value of the rate is reported in Column 2, systematic and statistical errors are in Columns 3 and 4 respectively. Column 5 contains the median number of supernova candidates in the samples used to calculate the weighted mean of the rate. Finally, we report the number of candidates used in each of the methods in Column 6.

TABLE 3 Compilation of volumetric supernova rates from the literature. Column 1 gives the minimum redshift, column 2 is the maximum redshift, column 3 is the average redshift, column 4 is the volumetric rate, column 5 is the systematic error, column 6 is the statistical error, column 7 is the number of SNe used in the measurement and column 8 contains the reference code (see footnote 4).

Min(z)	Max(z)	< z >	Rate[3]	Stat.	Syst.	N_{SN}	Reference[4]
0.0	0.0	0.0	2.8	$^{+0.9}_{-0.9}$		70	g,e
0.0	0.12	0.09	2.9	$^{+0.9}_{-0.7}$	$^{+0.2}_{-0.0}$	17	f
0.0	0.19	0.098	3.12	$^{+1.58}_{-1.58}$		19	h,e
0	0.2	0.1	5.69	$^{+0.98}_{-0.85}$	$^{+0.58}_{-0.47}$	52	p
0.0	0.3	0.13	2.0	$^{+0.7}_{-0.5}$	$^{+0.5}_{-0.5}$	14	e
0.02	0.2	0.14	3.43	$^{+2.7}_{-1.6}$	$^{+1.1}_{-0.6}$	4	i,e
0.0	0.5	0.25	0	$^{+2.4}_{-0.0}$		0	b
0.2	0.3	0.25	1.7	$^{+1.7}_{-1.7}$		1	n
0.18	0.37	0.25	2.86			1	j,e
0.3	0.4	0.35	5.3	$^{+2.4}_{-2.4}$		5	n
0.25	0.50	0.38	6.52			3	k,e
0.2	0.6	0.4	6.9	$^{+3.4}_{-2.7}$	$^{+15.4}_{-2.5}$	3	o
0.2	0.6	0.4	5.3	$^{+3.9}_{-1.7}$		5.44	a
0.4	0.5	0.45	7.3	$^{+2.4}_{-2.4}$		9	n
0.25	0.6	0.46	4.8	$^{+1.7}_{-1.7}$		8	l,e
0.2	0.6	0.47	8.0	$^{+3.7}_{-2.7}$	$^{+16.6}_{-2.6}$	8.8	c
0.2	0.6	0.47	4.2	$^{+0.6}_{-0.6}$	$^{+1.3}_{-0.9}$	73	d
0.25	0.85	0.55	5.4	$^{+0.74}_{-0.66}$	$^{+0.84}_{-0.82}$	37	m
0.5	0.6	0.55	20.4	$^{+3.8}_{-3.8}$		29	n
0.6	0.7	0.65	14.9	$^{+3.1}_{-3.1}$		23	n
0.5	1.0	0.75	4.3	$^{+3.6}_{-3.2}$		5.5	b
0.7	0.8	0.75	17.8	$^{+3.4}_{-3.4}$		28	n
0.6	1.0	0.8	15.7	$^{+4.4}_{-2.5}$	$^{+7.5}_{-5.3}$	14	o
0.6	1.0	0.8	9.3	$^{+2.5}_{-2.5}$		18.33	a
0.6	1.0	0.83	13.0	$^{+3.3}_{-2.7}$	$^{+7.3}_{-5.1}$	23.5	c
0.87	1.27	0.9	9.32			5	j,e
1.0	1.4	1.2	7.5	$^{+3.5}_{-3.0}$		8.87	a
1.0	1.4	1.2	11.5	$^{+4.7}_{-2.6}$	$^{+3.2}_{-4.4}$	6	o
1.0	1.4	1.21	13.2	$^{+3.6}_{-2.9}$	$^{+3.8}_{-3.2}$	20.2	c
1.0	1.5	1.25	10.5	$^{+4.5}_{-5.6}$		10.0	b
1.4	1.7	1.55	1.2	$^{+5.8}_{-1.2}$		0.35	a
1.4	1.8	1.6	4.4	$^{+3.2}_{-2.5}$	$^{+1.4}_{-1.1}$	2	o
1.4	1.8	1.61	4.2	$^{+3.9}_{-2.3}$	$^{+1.9}_{-1.4}$	3.1	c
1.5	2.0	1.75	8.1	$^{+7.9}_{-6.0}$		3.0	b

[3] 10^{-5}SNe $(Mpc/h_{70})^{-3}yr^{-1}$

[4] a) Kuznetsova et al. (2008), b) Poznanski et al. (2007), c) Dahlen et al. (2008), d) Neill et al. (2006), e) Blanc et al. (2004), f) Dilday et al. (2008), g) Cappellaro et al. (1999), h) Madgwick et al. (2003), i) Hardin et al. (2000), j) Gal-Yam et al. (2002), k) Pain et al. (1996), l)Tonry et al. (2003), m) Pain et al. (2002), n) Barris & Tonry (2006), o) Dahlen et al. (2004), p) This paper

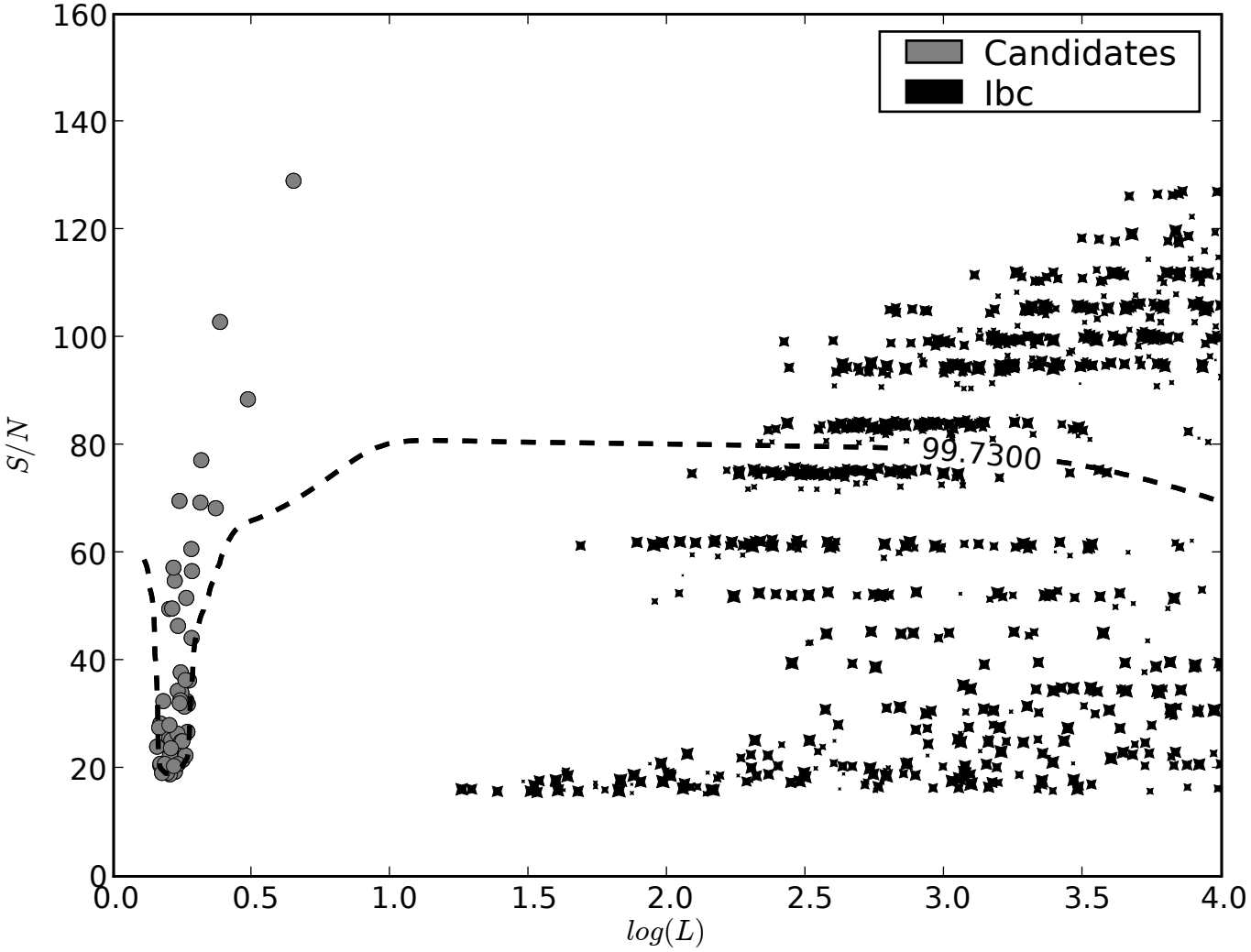
Candidates
Ibc
99.7300
S/N
log(L)
0
20
40
60
80
100
120
140
160
0.0
0.5
1.0
1.5
2.0
2.5
3.0
3.5
4.0

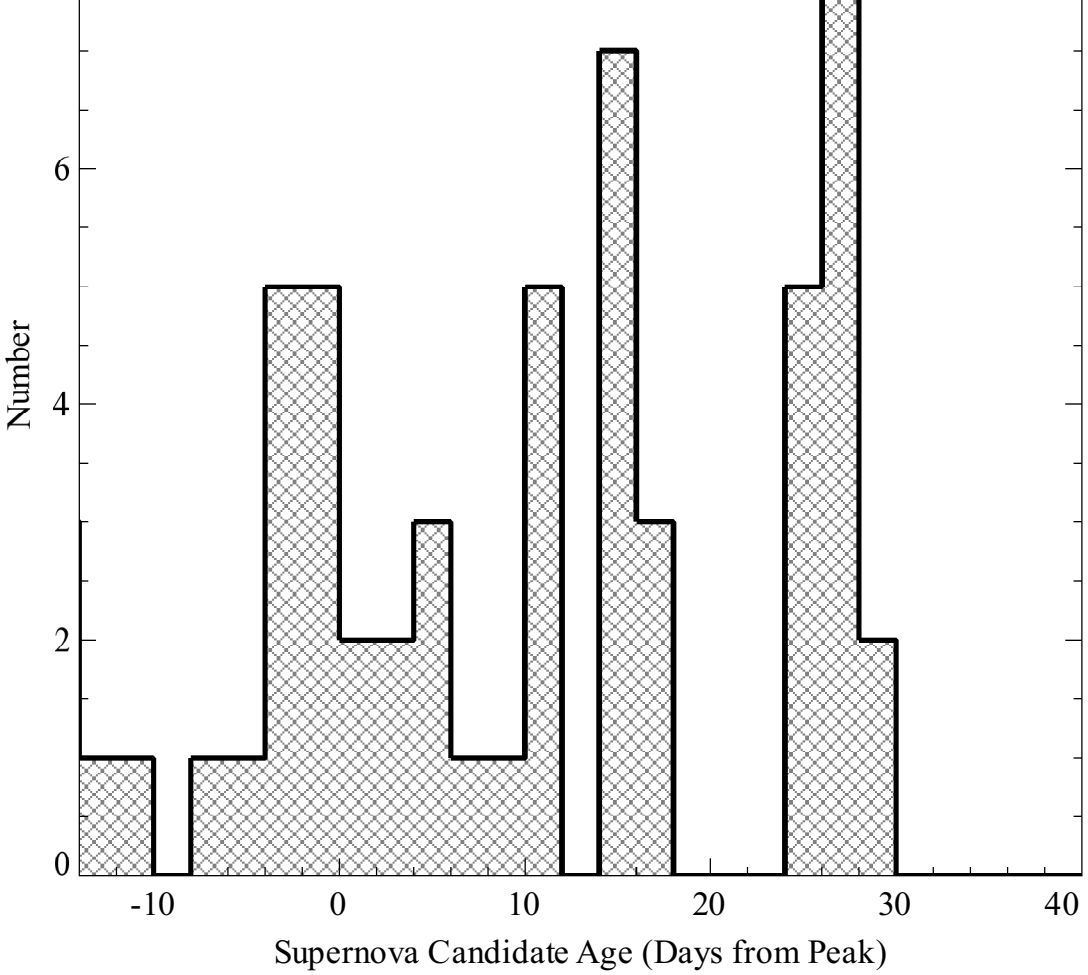
Number
0
2
4
6
-10
0
10
20
30
40
Supernova Candidate Age (Days from Peak)

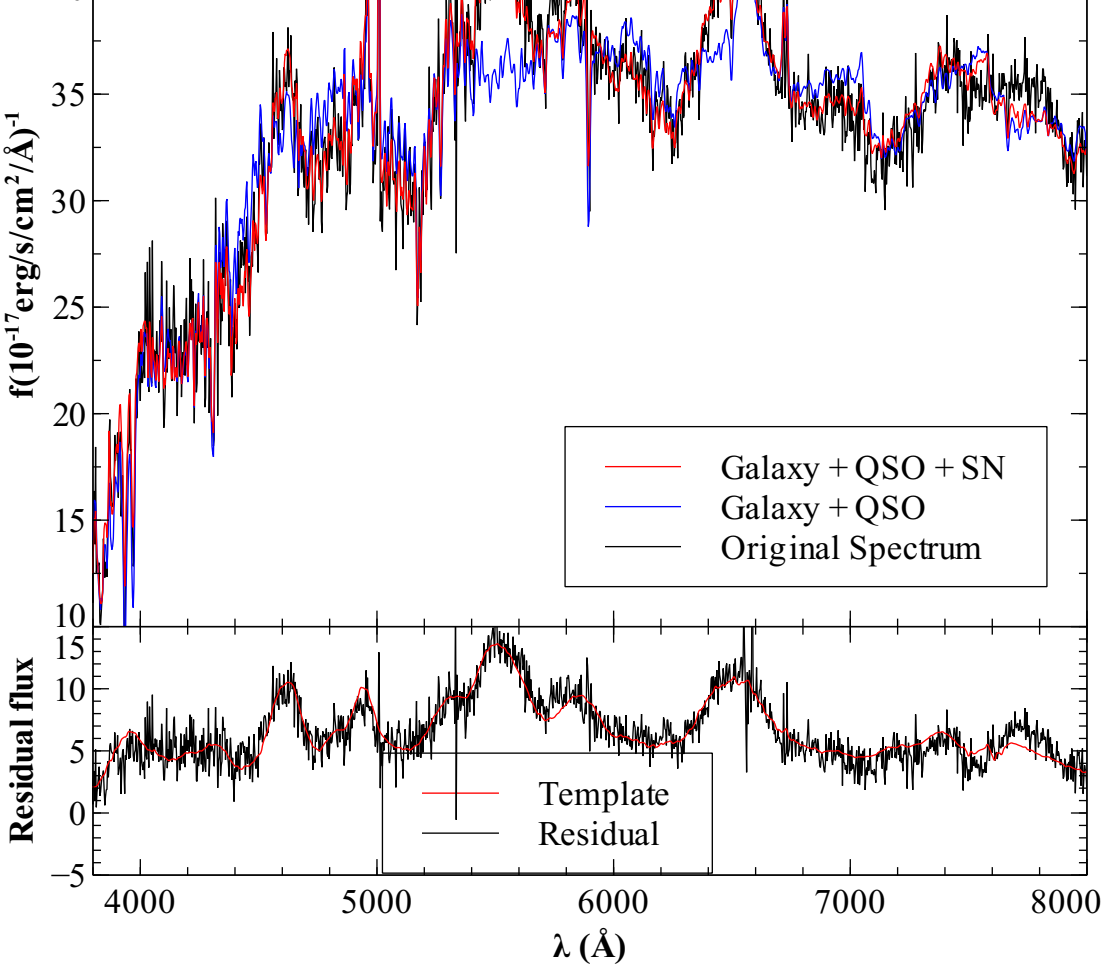
f(10^-17 erg/s/cm^2/Å)^-1
35
30
25
20
15
10
Galaxy + QSO + SN
Galaxy + QSO
Original Spectrum
Residual flux
15
10
5
0
−5
Template
Residual
4000
5000
6000
7000
8000
λ (Å)

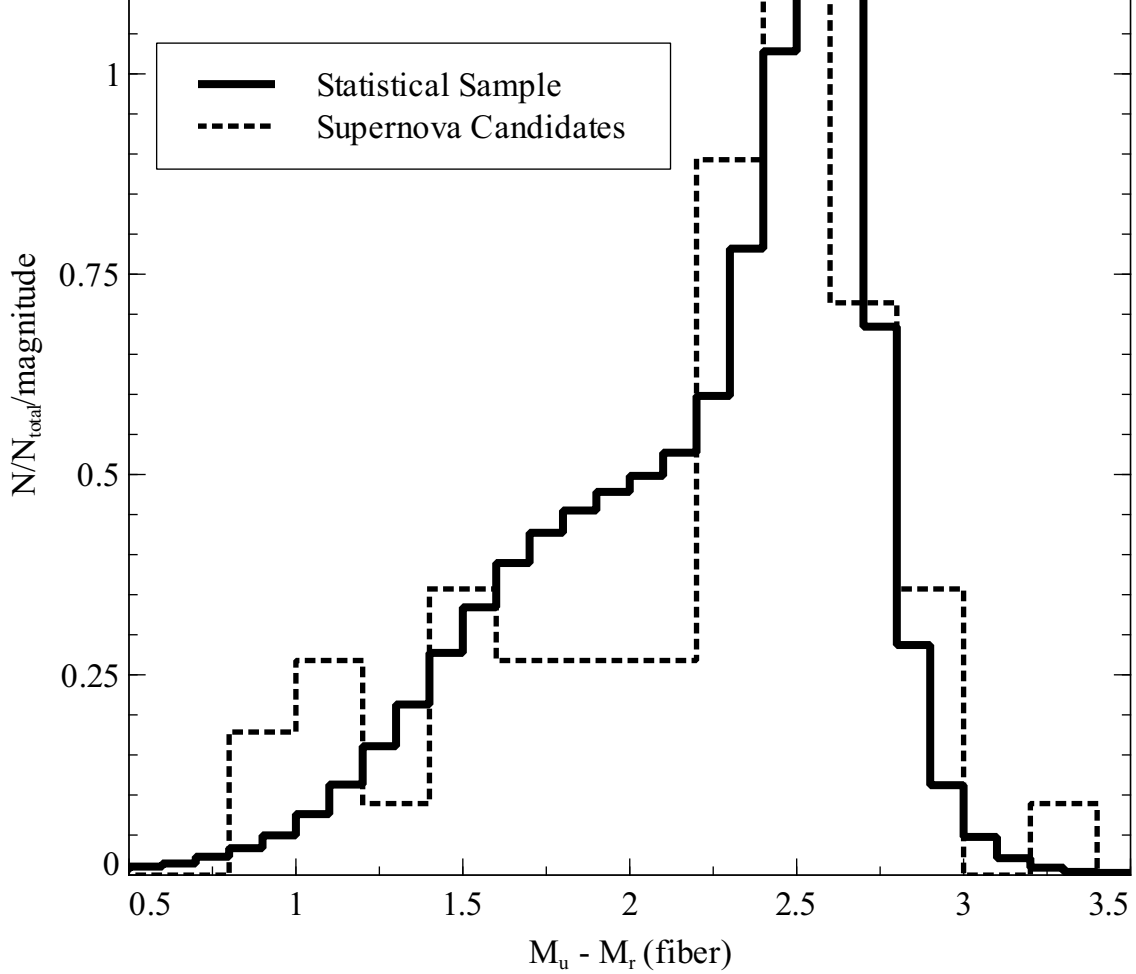
Statistical Sample
Supernova Candidates
N/N_total/magnitude
M_u - M_r (fiber)
0
0.25
0.5
0.75
1
0.5
1
1.5
2
2.5
3
3.5

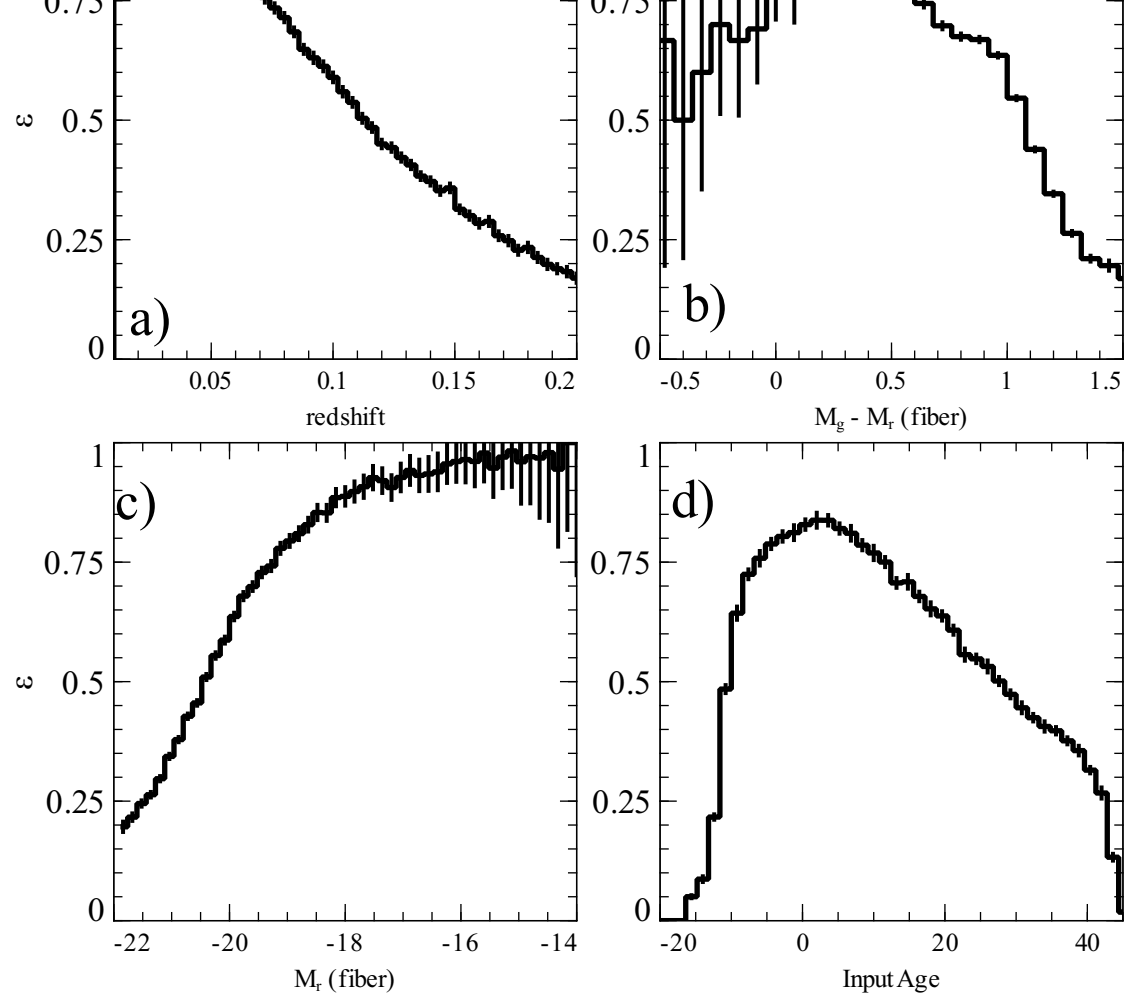
a)
b)
c)
d)
ε
redshift
M_g - M_r (fiber)
M_r (fiber)
Input Age

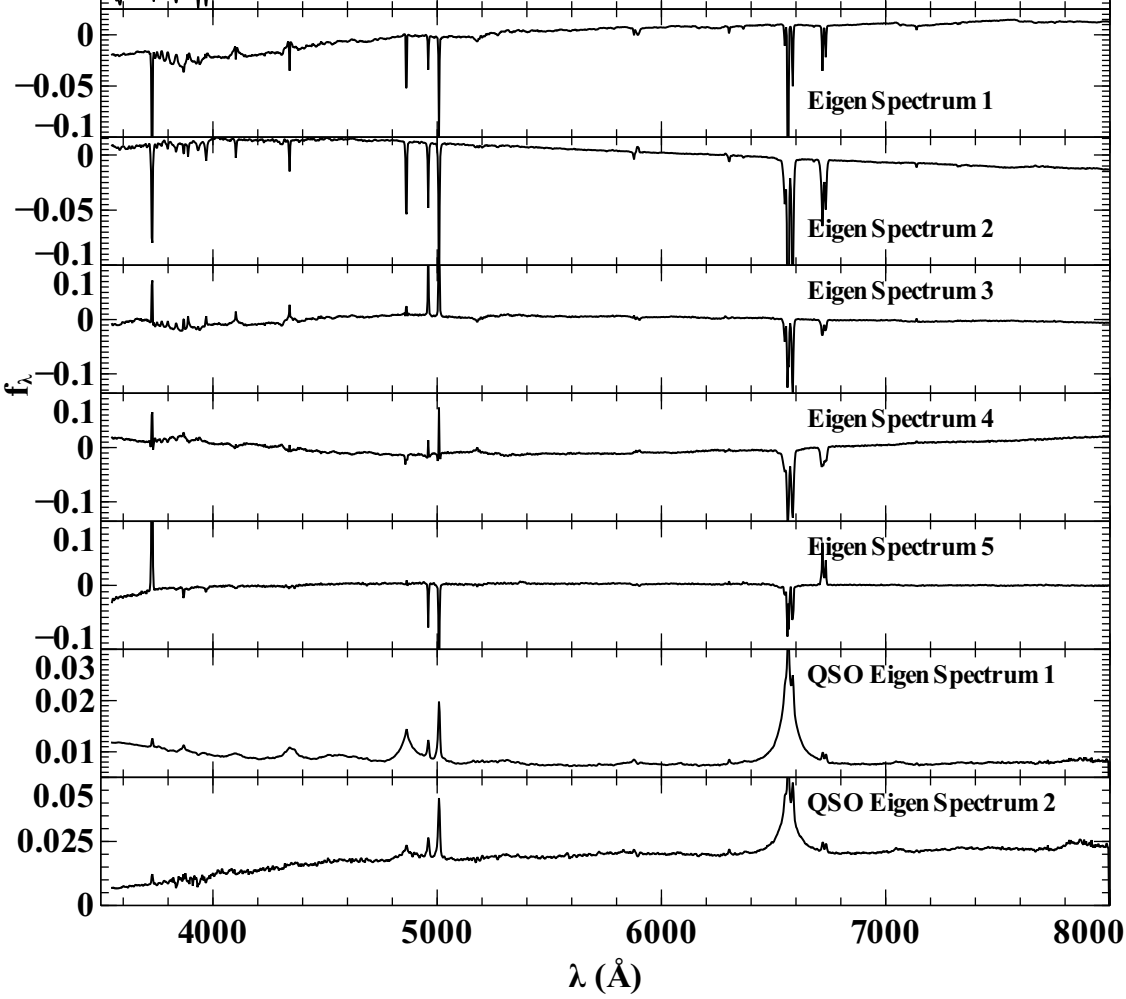
Eigen Spectrum 1
Eigen Spectrum 2
Eigen Spectrum 3
Eigen Spectrum 4
Eigen Spectrum 5
QSO Eigen Spectrum 1
QSO Eigen Spectrum 2
f_λ
λ (Å)
4000
5000
6000
7000
8000

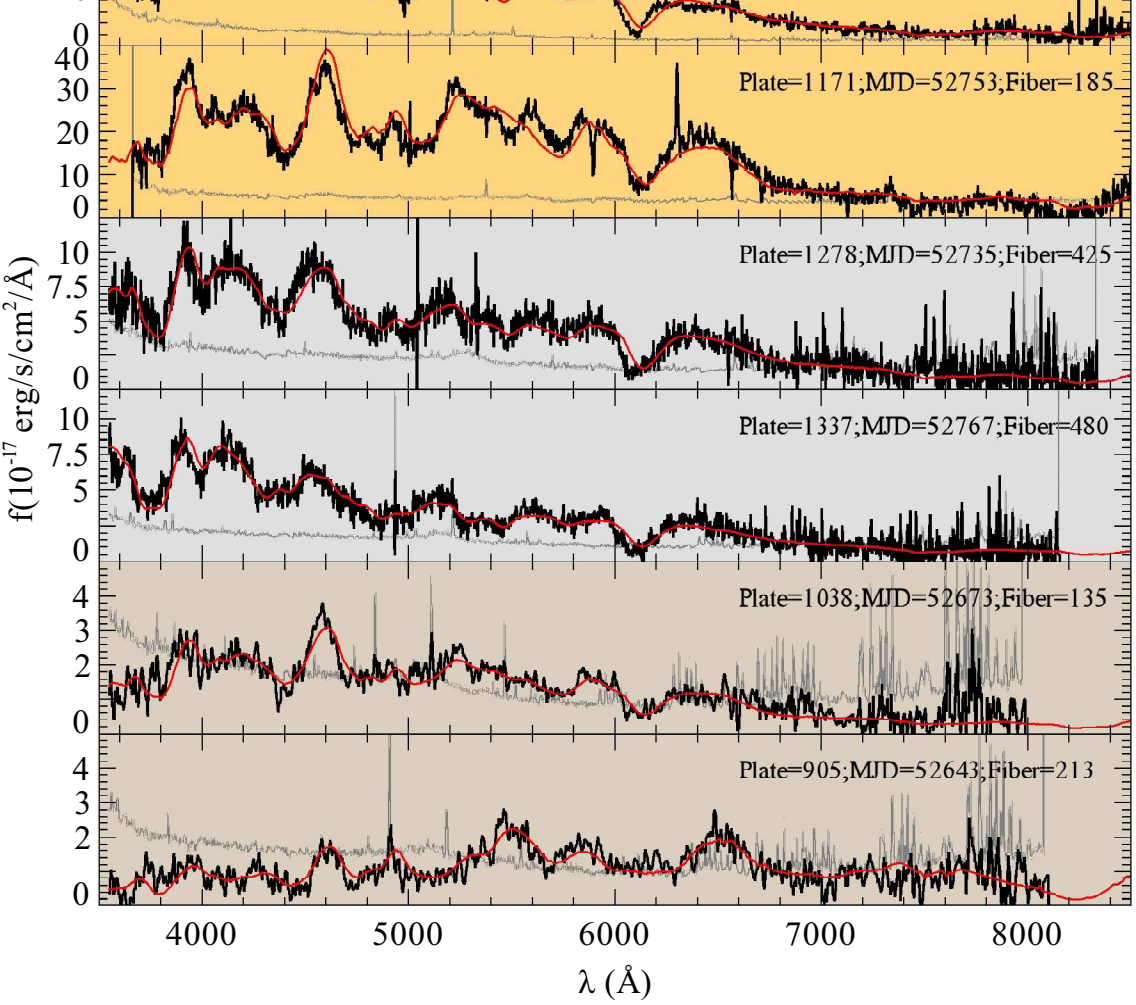
Plate=1171;MJD=52753;Fiber=185
Plate=1278;MJD=52735;Fiber=425
Plate=1337;MJD=52767;Fiber=480
Plate=1038;MJD=52673;Fiber=135
Plate=905;MJD=52643;Fiber=213
f(10^-17 erg/s/cm^2/Å)
λ (Å)
4000
5000
6000
7000
8000

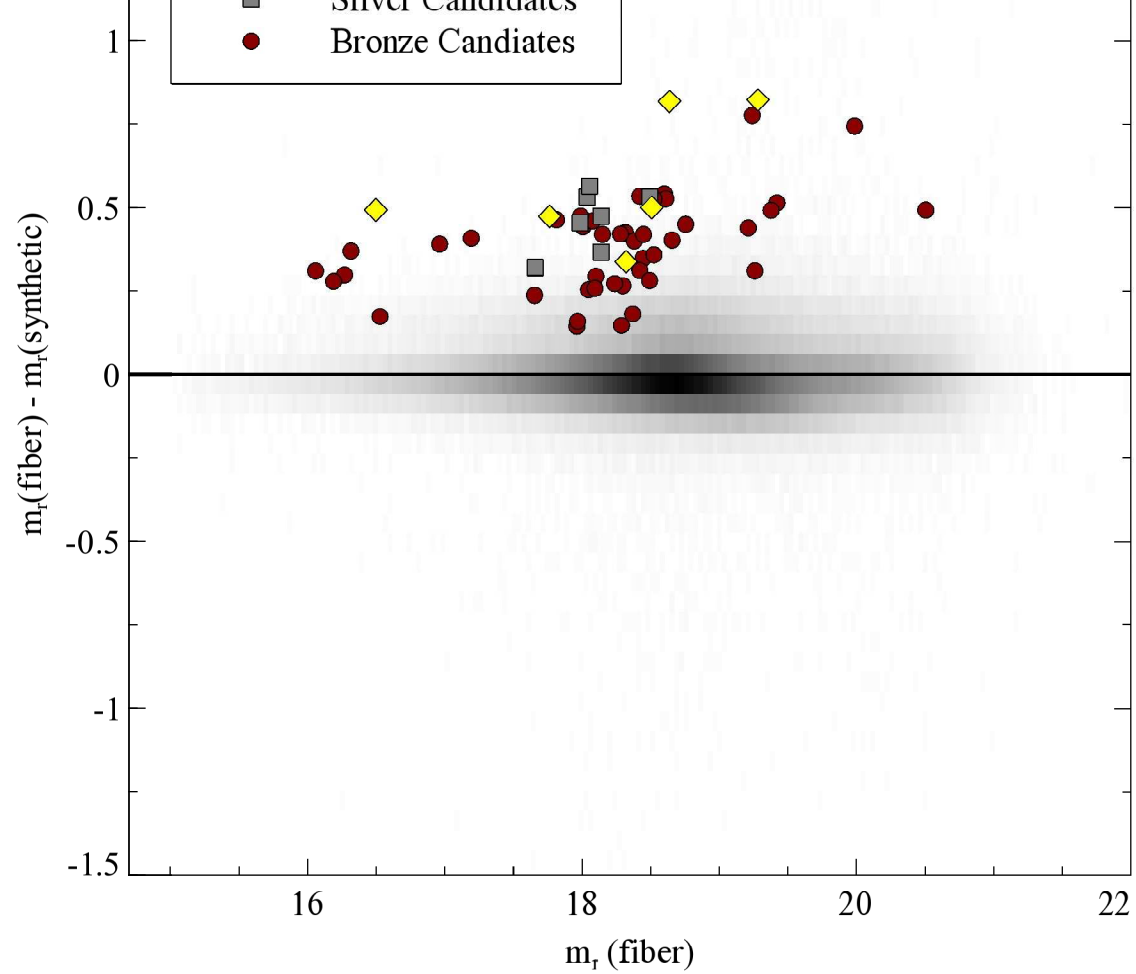
Silver Candidates
Bronze Candidates
1
0.5
0
-0.5
-1
-1.5
16
18
20
22
m_r(fiber) - m_r(synthetic)
m_r (fiber)

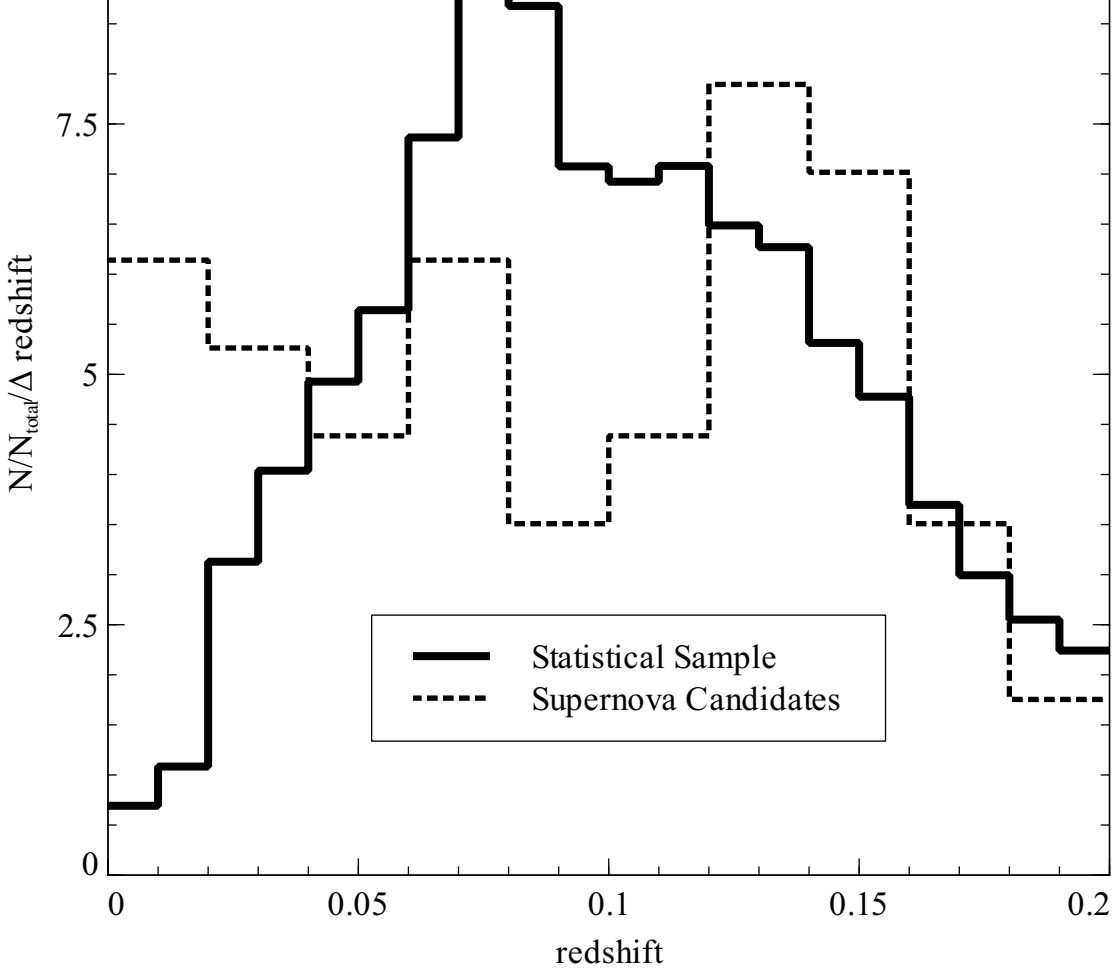
7.5
5
2.5
0
N/N_total/Δ redshift
0
0.05
0.1
0.15
0.2
redshift
Statistical Sample
Supernova Candidates

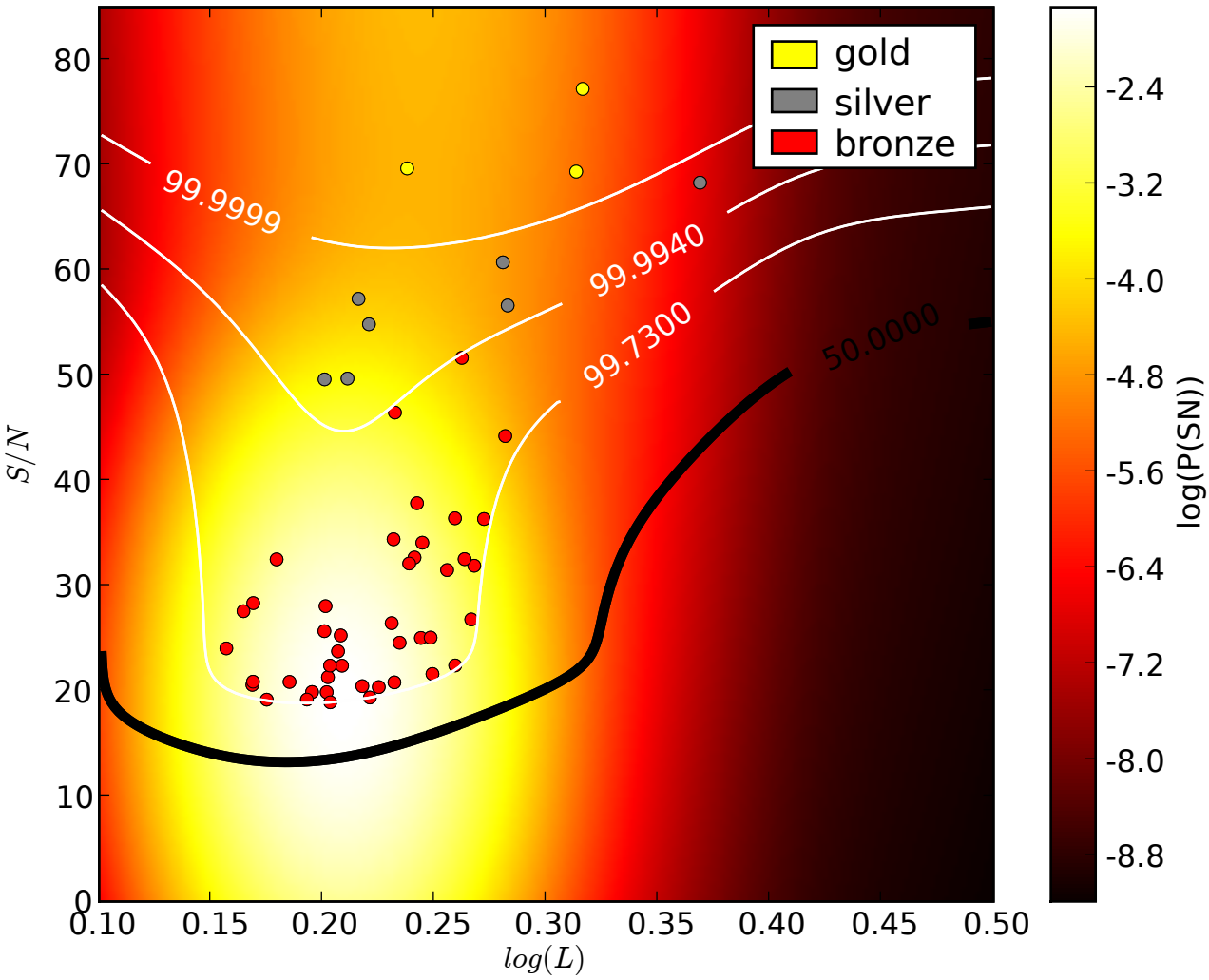
gold
silver
bronze
99.9999
99.9940
99.7300
50.0000
S/N
log(L)
log(P(SN))
0
10
20
30
40
50
60
70
80
0.10
0.15
0.20
0.25
0.30
0.35
0.40
0.45
0.50
-2.4
-3.2
-4.0
-4.8
-5.6
-6.4
-7.2
-8.0
-8.8

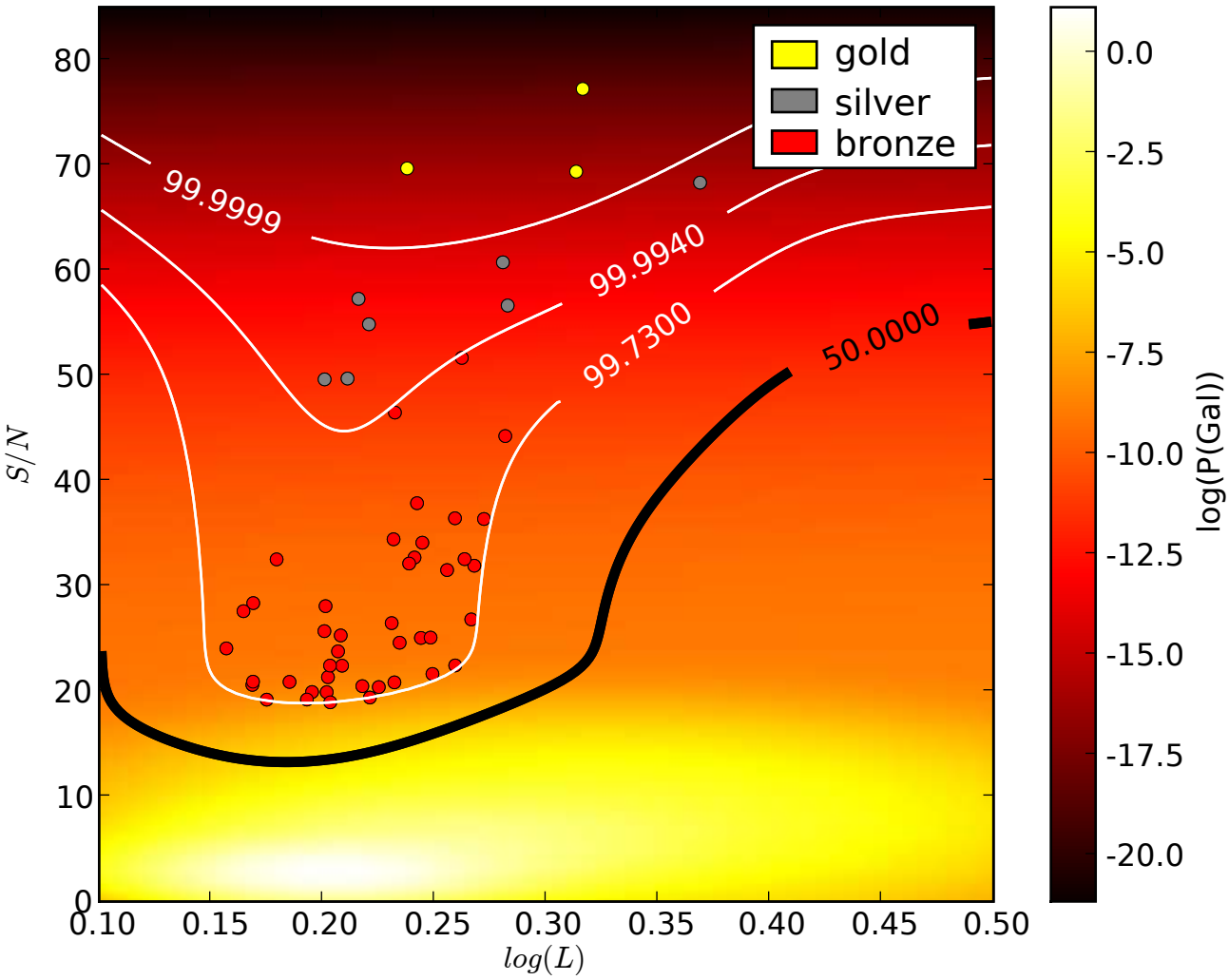
gold
silver
bronze
99.9999
99.9940
99.7300
50.0000
S/N
log(L)
log(P(Gal))
0
10
20
30
40
50
60
70
80
0.10
0.15
0.20
0.25
0.30
0.35
0.40
0.45
0.50
0.0
-2.5
-5.0
-7.5
-10.0
-12.5
-15.0
-17.5
-20.0

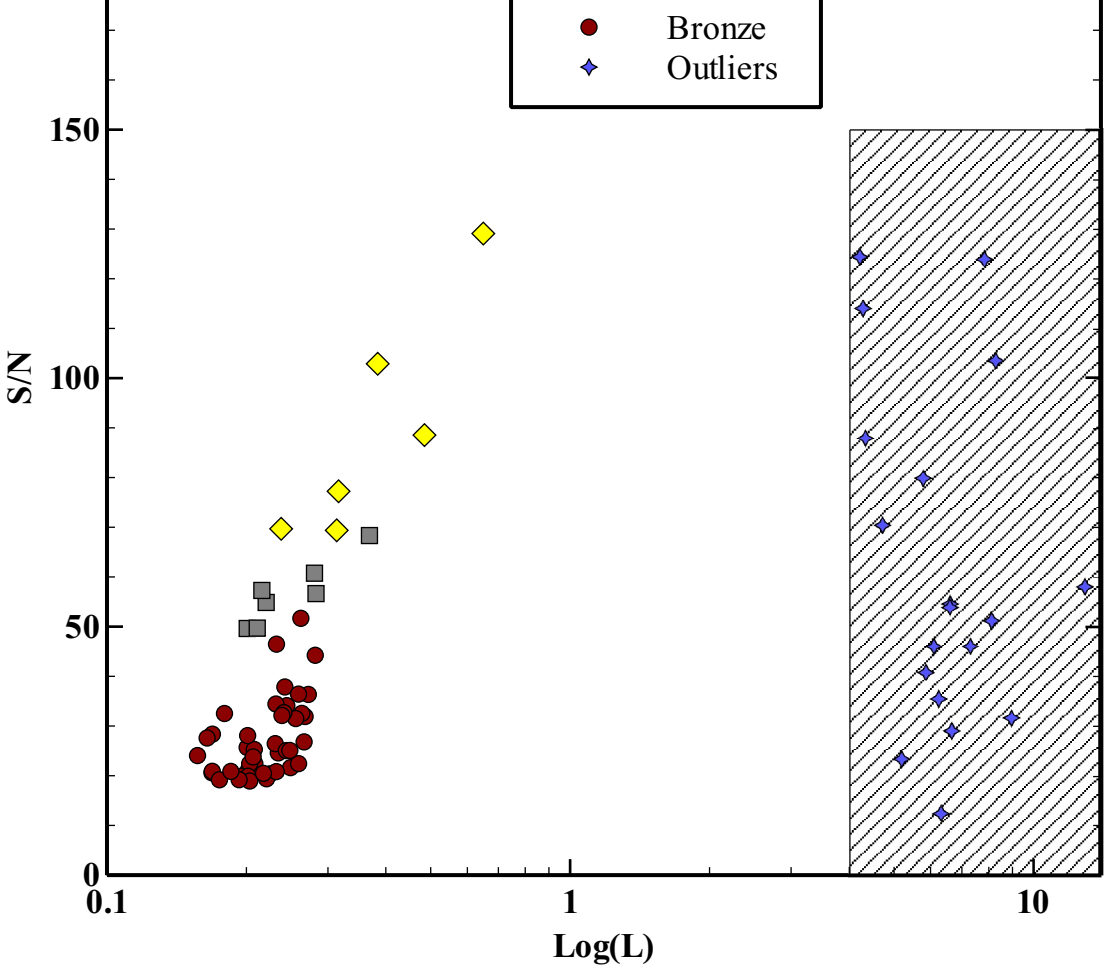
Bronze
Outliers
150
100
50
0
S/N
0.1
1
10
Log(L)

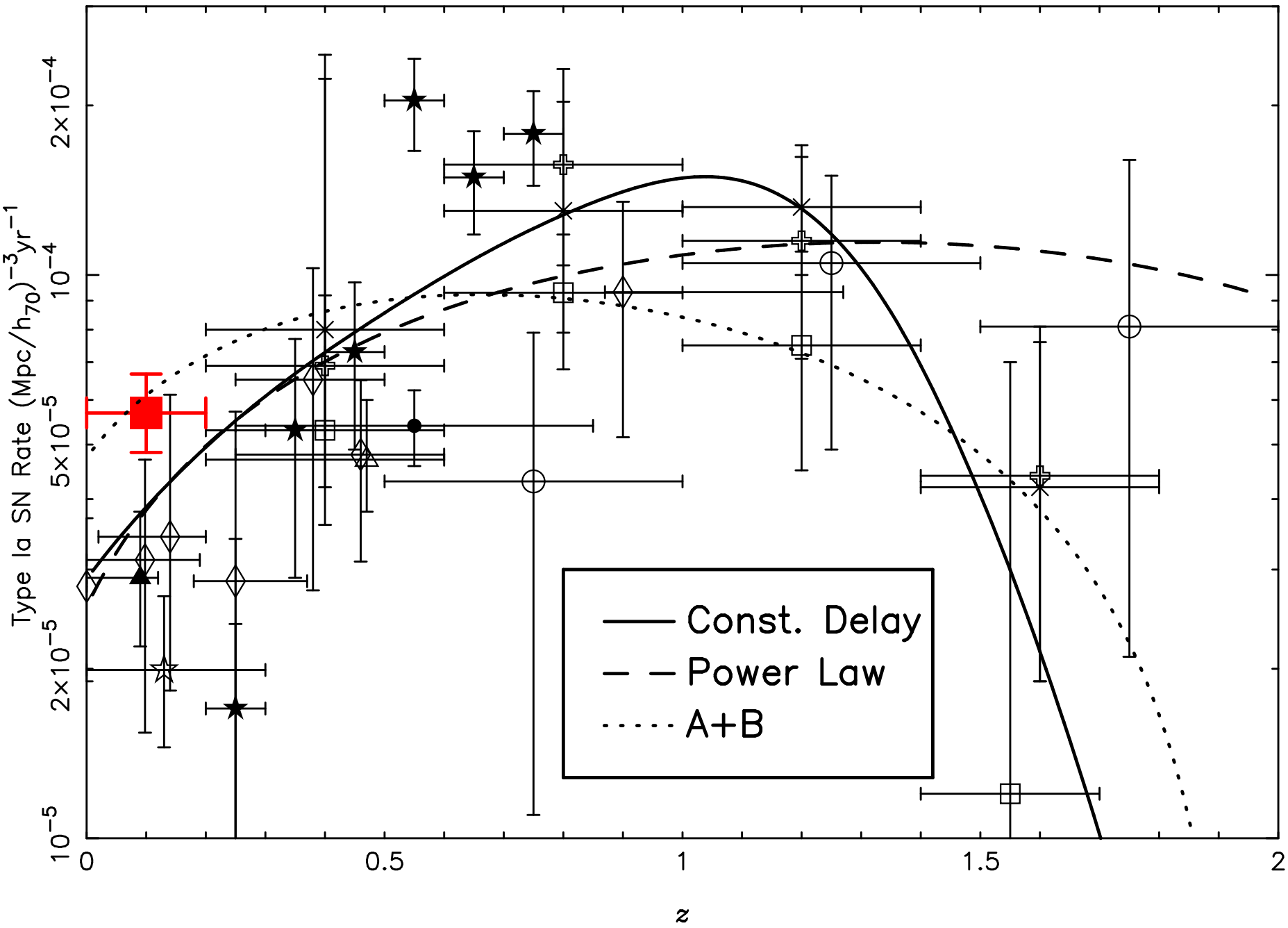
Type Ia SN Rate (Mpc/h$_{70}$)$^{-3}$yr^{-1}
2×10^{-4}
10^{-4}
5×10^{-5}
2×10^{-5}
10^{-5}
0
0.5
1
1.5
2
z
Const. Delay
Power Law
A+B

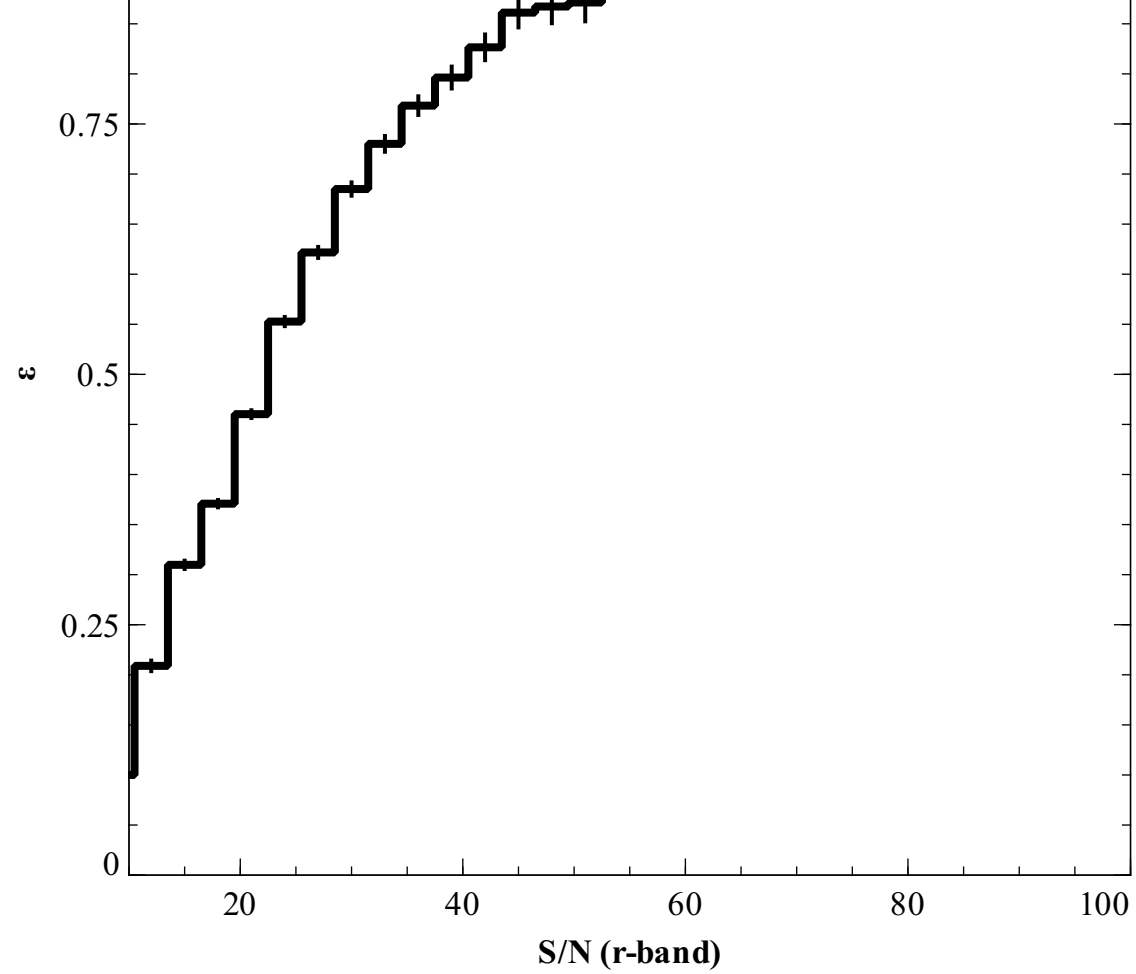
0.75
0.5
0.25
0
ε
20
40
60
80
100
S/N (r-band)

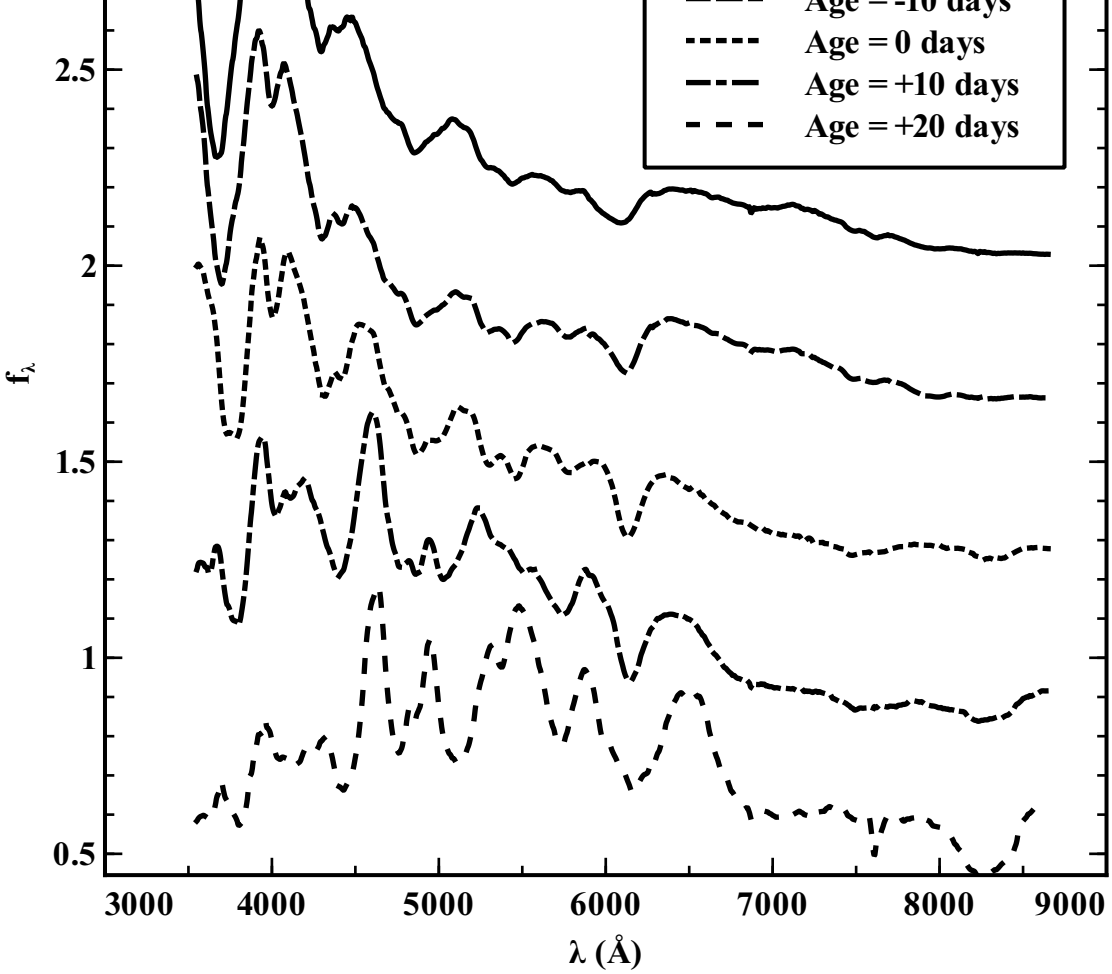
Age = -10 days
Age = 0 days
Age = +10 days
Age = +20 days
f_λ
λ (Å)
0.5
1
1.5
2
2.5
3000
4000
5000
6000
7000
8000
9000

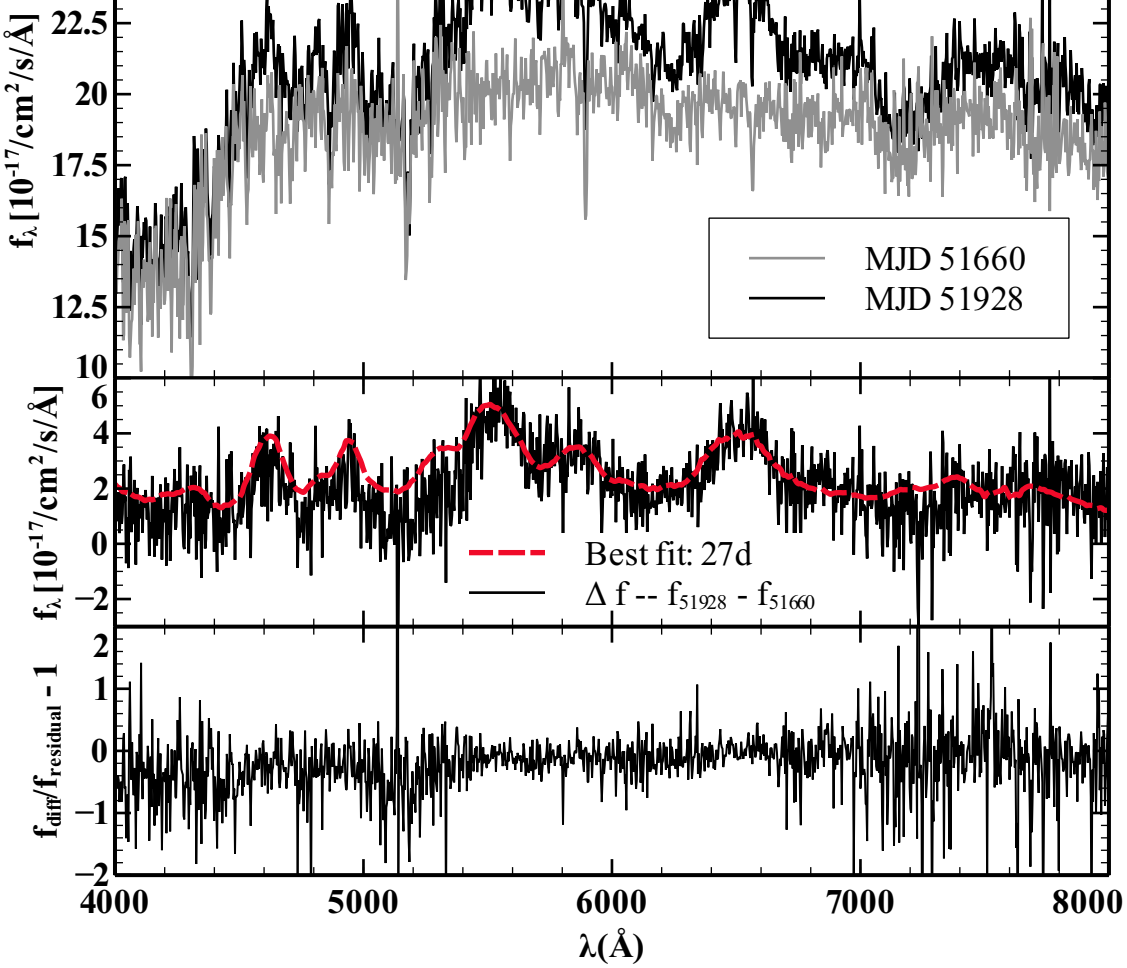
MJD 51660
MJD 51928
Best fit: 27d
Δ f -- f51928 - f51660
fλ [10-17/cm2/s/Å]
fdiff/fresidual - 1
λ(Å)